# Comparison of individual-based model output to data using a model of walleye pollock early life history in the Gulf of Alaska.

S. Hinckley[a,1], C. Parada[b,c], J. K. Horne[d], M. Mazur[e], M. Woillez[f]

[a]*Alaska Fisheries Science Center, 7600 Sand Point Way, NE, Seattle, 98115.*

[b]*Departamento de Geofísica, Universidad de Concepción, Chile. Email: carolina.parada@dgeo.udec.cl*

[c]*Instituto Milenio de Oceanografía (IMO),Universidad de Concepción, Chile.*

[d]*School of Aquatic and Fisheries Science, University of Washington, Box 355020 Seattle, WA 98195-5020. Email: jhorne@u.washington.edu*

[e]*U.S. Fish & Wildlife Service, 170 North First Street, Lander, Wyoming 82520. Email: michael_mazur@fws.gov*

[f]*IFREMER, Sciences et Technologies Halieutiques, Brest, France. Email: mathieu.woillez@gmail.com*

For submission to: GOAIERP Special Issue I of Deep Sea Research II

[1]Corresponding Author. Tel: 1-206-658-5551. Email: sarah.hinckley@noaa.gov.

**Abstract**

Biophysical individual-based models (IBMs) have been used to study aspects of early life history of marine fishes such as recruitment, connectivity of spawning and nursery areas, and marine reserve design. However, there is no consistent approach to validating the spatial outputs of these models. In this study, we hope to rectify this gap. We document additions to an existing individual-based biophysical model for Alaska walleye pollock (*Gadus chalcogrammus*), some simulations made with this model and methods that were used to describe and compare spatial output of the model versus field data derived from ichthyoplankton surveys in the Gulf of Alaska. We used visual methods (e.g. distributional centroids with directional ellipses), several indices (such as a Normalized Difference Index (NDI), and an Overlap Coefficient (OC), and several statistical methods: the Syrjala method, the Getis-Ord Gi* statistic, and a geostatistical method for comparing spatial indices. We assess the utility of these different methods in analyzing spatial output and comparing model output to data, and give recommendations for their appropriate use. Visual methods are useful for initial comparisons of model and data distributions. Metrics such as the NDI and OC give useful measures of co-location and overlap, but care must be taken in discretizing the fields into bins. The Getis-Ord Gi* statistic is useful to determine the patchiness of the fields. The Syrjala method is an easily implemented statistical measure of the difference between the fields, but does not give information on the details of the distributions. Finally, the geostatistical comparison of spatial indices gives good information of details of the distributions and whether they differ significantly between the model and the data. We conclude that each technique gives quite different information about the model-data distribution comparison, and that some are easy to apply and some more complex. We also give recommendations for a multistep process to validate spatial output from IBMs.

Keywords: Mathematical Models, Statistical analysis, Marine fish, Spatial distributions, Spatial Analysis, Individual-based Models, USA Gulf of Alaska, Walleye pollock

## 1.1 **Introduction**

Model validation (i.e. the comparison of model output to external, independently derived data) is a necessary part of the development and use of ecological models. Individual-based biophysical models (IBMs) of larval fish dispersal and early life history have been used in fisheries for several decades, but are often not well validated; there is much room for improvement (North et al, 2009). Depending on the purpose of the model, the type of validation will differ. In drift and connectivity studies, the emphasis is on validating spatial distributions and trajectories of larvae. Investigations examining growth, mortality and recruitment will need different types of validation; these are not discussed here. Spatial outputs of biophysical individual-based models are often compared to data by placing maps side-by-side for the reader, which is a good first step, but it is not quantitative. Several measures or indices have been used to compare individual-based model spatial outputs to empirical data, however there has been no consistent approach using multiple methods.

There are limited methods that can be used validate model predictions of larval dispersal and transport of individuals. One method compares trajectories from model predictions to those from satellite-tracked drifters (North et al. 2009). This comparative method is usually based on a relatively limited numbers of drifters that were deployed at fixed depths, incorporate wind effects, and adds cost to the model validation. Characteristics of drifters predispose satellite-tracked drifter tracks to diverge from larval fish trajectories, such as the effect of wind on the drifter, or use of a constant depth of the drogue when individual fish often move vertically in the water column.

An alternative approach could be to use uniquely marked individual animals. Chemical marking has been attempted (North et al. 2009), and might be a useful validation technique but is only applicable when populations are small, mortality is low, and the likelihood of recapture is reasonable. Elemental fingerprinting has been used to infer natal origin of animals captured during distribution and abundance surveys (Thorrold et al. 2001, DiBacco and Levin 2000, Zacherl et al. 2003, Becker et al. 2007), and might be used to validate individual-based model (IBM) connectivity between spawning and nursery grounds, but detectable differences in seawater trace elemental composition between sites is required, and still, actual trajectories remain unknown. The

88 required gradient and resolution to detect change among sites may vary with factors other
89 than seawater composition (e.g. temperature, salinity), and it adds cost to the validation.
90 The use of otolith microchemistry enables assessment of larval fish natal origin
91 (Campana, 1999; Thorrold et al., 2001), and seascape genetics or genetic fingerprinting
92 may be used in some situations (Coscia et al., 2013, Selkoe et al., 2008, Galindo et al.
93 2010, Palumbi, 2003), but source populations must be known and characterized by
94 detectable genetic differences (Hedgecock et al., 2007). Model error quantification
95 techniques used for hydrodynamic models include cost functions (Delhez *et al.*, 2004;
96 Radach and Moll, 2006), root-mean-square error of modeled vs. observed values, model
97 skill scores (Warner et al., 2005), and Taylor diagrams (Taylor, 2001).
98 One of the most straightforward ways to validate dispersal and transport IBMs is
99 by comparing modeled spatial distributions with empirical distributions of larvae and
100 juveniles. Although it cannot be known if individuals from spawning sites are the same
101 individuals that are caught during surveys, this comparative approach can be useful when
102 the sources of individuals caught in the field are relatively well known. Several studies
103 using IBMs have used several different measures to analyze spatial distributions (overlap
104 index, Hinrichsen et al. 2005, Morisita's simplified overlap index, Utne and Huse, 2012,
105 centroids (center of gravity), Vikebø et al. 2005, Castaño-Primo et al. 2014, (defined as
106 convex hull), Petrik et al. 2014 and Utne and Huse 2012, Jaccard's Coefficient,
107 Weidmann et al., 2012, a Correlation Index based on linear regression, Pedersen, et al.
108 2009, Root Mean Square Deviation (RMSD), Utne and Huse, 2012), the local index of
109 collocation (Petrik et al, 2014), but no comparison of methods has been published.
110 We use walleye pollock (*Gadus chalcogrammus*) in the Gulf of Alaska (GOA) as
111 a case study to validate the spatial output from an individual-based dispersal model.
112 Walleye pollock has been studied intensively for several decades, and many lab studies
113 and field surveys have been done. We used 1987 as our test year in this study, as there
114 were several sequential surveys of different early life stages done in that year. Walleye
115 pollock in the Gulf of Alaska have a life history where spawning and nursery habitat
116 appear to be spatially disaggregated, and most of the currents in the region where pollock
117 spawn are highly advective. Historically, a large part of the egg production of pollock
118 has been located at the southwestern entrance to Shelikof Strait, an area between Kodiak

Island and the Alaska Peninsula (Fig. 1, Kendall et al., 1987; Schumacher and Kendall, 1991). Pollock eggs are spawned between mid-March and early May, with spawning peaking at the beginning of April (Doyle and Mier, This issue). By May, larvae are advected southwest by the Alaska Coastal Current (ACC) along the Alaska Peninsula. By summer and through early fall, juveniles arrive at their primary nursery area in the vicinity of the Shumagin Islands (Hinckley et al., 1991; Spring and Bailey 1991; Wilson et al., 1996; Hinckley et al., 2001). Other potential spawning and nursery areas have been reported in the literature (Wilson, 2000; Bailey et al., 1999; Mazur et al., 2007), but their relative contribution to the recruitment of pollock in the GOA is not known, nor is how their contributions may have changed over time. Spatial and temporal variability in spawning and the variability of current patterns may determine which locations function as pollock nursery habitats in the GOA, and explain some of the variability in pollock abundance. Connectivity between spawning and nursery areas is important to understanding recruitment, as differentiating between possible sub-populations is needed to clarify stock management areas.

A biophysical model, consisting of an IBM coupled with a hydrodynamic model, has been used to assess pollock spawning-nursery area connectivity in the GOA (Parada et al., This issue). The spatially-explicit features of biophysical models and the Lagrangian approach enable tracking of particles representing individuals from spawning area release locations to nursery destinations as juveniles. The work described here extends previous work that explored the life history of walleye pollock (Hinckley et al. 1996, Hinckley et al. 2001, Megrey and Hinckley, 2001, Hermann et al. 2001).

In this study, we update the IBM for pollock, and compare methods to validate modeled spatial distributions. Our goal is to see if this biophysical model can reproduce observed distributions of early life stages of walleye pollock between early larvae in the spring and juveniles in September. Spatial and temporal matches between model outputs and observed distributions will be compared using multiple methods. This will enable evaluation of various techniques which could be used to validate IBM outputs, and increase understanding of walleye pollock early life history.

## 2.1 **Methods**

The individual based biophysical model we use for walleye pollock has been described in detail elsewhere (Hinckley et al., 1996, Megrey and Hinckley, 2001). Here we give an overview of the model, and describe additions and updates to the model in detail.

### 2.1.1 The Walleye Pollock Individual-based Model

The pollock IBM, originally developed by S. Hinckley, B. Megrey and A. Hermann, simulates four developmental stages (eggs, yolk-sac larvae, feeding larvae, and juveniles) of 0-age pollock from spawning to the autumn of their spawning year. Processes in the model are stage-dependent (Hinckley et al., 1996; Megrey and Hinckley 2001). Egg development was driven by age and temperature (Blood et al., 1994). Yolk-sac larval growth depended on degree days which were accumulated for every day after hatch using temperature information from the physical model for each location and time step. A feeding probability for yolk-sac larvae was calculated prior to entering the feeding larval stage, unless they passed the point of no return without feeding, in which case they died. Dry weight of feeding larvae and juveniles depended on consumption (a function of individual weight and temperature, as described in Hinckley et al. 1996) and a bioenergetics formulation. The bioenergetics submodel for larvae included assimilation efficiency (Houde, 1989) and daily respiration rate (Yamashita and Bailey, 1989), and for juveniles, was estimated according to a modified version of Ciannelli et al.'s model (1998, see below) model. Net growth in weight (g) of larvae and juveniles was updated at each time step and converted to growth in length (mm).

Superindividual schemes (Scheffer et al., 1995, Megrey and Hinckley, 2001, Bartsch and Coombs, 2004) are approaches that allow the use of realistic mortality rates in IBMs by increasing the number of individuals represented by each particle (i.e. superindividual). In this way, we can simulate larger numbers of fish in a population without adding to computer processing time. The assumption behind this approach is that growth, feeding conditions, and the probability of mortality for each individual within a superindividual are the same (as they are at the same location). At the beginning of the simulation, each superindividual is assigned a "count", indicating how many individual

fish the superindividual represents. This "count" is decreased by applying a random deviate from the daily mortality rate for that particular life stage. At any point in time, the total number of fish is the sum of the "count" variable over all superindividuals.

The daily probability of mortality for eggs, yolk-sac larvae, feeding larvae and juveniles in the pollock model was given by an exponential function dependent on the instantaneous daily mortality rate of the respective stage. We assumed that each particle represented a cohort of pollock eggs released in the spawning areas. The number of surviving superindividuals was assessed at each time step.

Each cohort of superindividuals was assigned to a particle that moved according to the directional ($u$,$v$ and $w$) components of velocity following a Lagrangian trajectory, plus behavioral subroutines that differed by life stage. Particle tracking was based on the Euler method, and we used a Java tool developed by Lett et al. (Ichthyop, 2008) which used the Regional Ocean Modeling System (ROMS, see below) native grid. The unique trajectories of the particles integrated environmental conditions experienced by each individual. Each trajectory resulted in a unique pattern of growth, distribution, and survival.

Algorithms for particle depth were stage dependent, as in Hinckley et al. (1996). The vertical position of each egg was calculated at each time step and depended on the terminal velocity (based on the density of the egg at each developmental stage) and the vertical component of water velocity, $w$, from the ROMS model. The terminal velocity was calculated based on Sundby (1983). Parameters for calculating changes in egg vertical location are described in Hinckley et al. (1996). Yolk-sac larvae were assumed to remain at the depth of hatch until first-feeding. Feeding larvae rose to the upper water column and began diel migrations at 6 mm with swimming speeds a function of length (Kendall et al., 1987; 1994). Larvae were found at the deepest level during midday and at the shallowest depth at dusk. They were found somewhat deeper at night than at dusk or at dawn. Vertical and horizontal movements of juveniles are described below.

### 2.1.2 Additions to the Pollock Model

The following are additions to the original pollock IBM of Hinckley et al (1996) and Megrey and Hinckley (2001).

212

213 2.1.2.1 Growth and Bioenergetics of 0-age Juveniles

214 A Gerritsen and Strickler (1977) encounter model as simplified by Evans (1989),
215 was adapted for the juvenile stage of this model, and used to calculate the number of each
216 prey type encountered by feeding juvenile pollock per hourly time interval (Eggers,
217 1977). We assumed the visual field of foraging juveniles was uniform within the search
218 volume and did not attempt to account for microhabitat differences in the position of prey
219 within the visual field (Mazur and Beauchamp 2006). Reaction distance was set at a
220 constant distance for feeding during lighted periods; juvenile pollock were only allowed
221 to feed during light periods of the diel cycle. Diel observations of juvenile pollock
222 consumption *in situ* suggested little feeding occurs outside of lighted periods of the day
223 (Mazur et al. 2007).

224 Prey consumption of juveniles was estimated using a bioenergetics-based
225 foraging model for planktivorous fish (Tables 1, 2) developed by Bevelhimer and Adams
226 (1993), evaluated by Stockwell and Johnson (1997), and subsequently field tested
227 (Stockwell and Johnson 1999). For a full description of this modeling approach see
228 Eggers (1977) and Stockwell and Johnson (1997, 1999). A similar approach was recently
229 utilized to investigate pollock recruitment variability in the Eastern Bering Sea (Siddon et
230 al. 2013). Estimates of prey consumption per hourly time step were generated using a
231 single-species functional response that was modified to use prey encounters rather than
232 weight (Bevelhimer and Adams 1993, Stockwell and Johnson 1997). The prey field used
233 in the model was based on the horizontal distribution of euphausiids, large copepods and
234 small copepods from an NPZ model described in Hinckley (1999), for the inner shelf, the
235 mid and outer shelf, and the offshelf areas. Prey preferences were set following Wilson
236 et al. (2006). Consumption of each prey type was partitioned based on juvenile pollock
237 body size and prey size and summed to estimate the total number of each prey type
238 potentially available for consumption per hour. Prey consumption was not allowed to
239 exceed the theoretical maximum daily consumption (Cmax) for pollock of each size as
240 estimated by the bioenergetics model (Ciannelli et al. 1998, Hansson et al. 1996).
241 Consumption of prey during each hourly time step only occurred when space was
242 available in the stomach following digestion and the daily maximum had not been

243 reached or exceeded. Daily maximum feeding rates were reset following the dark “no
244 feeding” period of each diel cycle.
245 A new submodel for the bioenergetics of juvenile pollock was implemented in
246 this IBM based on a modified version of Ciannelli et al.’s, (1998) model (Table 2). The
247 energy consumed and subsequently digested (D) in the model was allocated between
248 metabolism (R), egestion (F), excretion (U) and growth (G) (Hewett and Johnson, 1992):
249 G = D-R-F-U
250 Digestion was modeled hourly (Elliott and Pearson 1978) and used evacuation
251 rates estimated for juvenile pollock (Merati and Brodeur 1996, Mazur et al. 2007).
252 Numbers of each potential prey type were converted to weights and allowed to enter the
253 diet based on available stomach capacity and prey preference. Growth of juvenile
254 pollock was estimated using the bioenergetics model and the amount of available prey
255 energy digested on an hourly time step (Stockwell and Johnson 1997). Prey energy
256 density estimates for the Gulf of Alaska can be found in Mazur et al. (2007). Estimates of
257 growth in weight (g) were updated each time step and converted to growth in length
258 (mm) for use in subsequent foraging model time steps.
259
260 2.1.2.2 Predation on Juveniles
261 Groundfish predation on 0-age juveniles was added to the juvenile subroutine.
262 Other sources of predation (seabirds, marine mammals) on pollock can be important,
263 however, comprehensive data with enough spatial and temporal resolution, plus
264 consumption rates, do not exist. Predation rates were based on 8 years of groundfish
265 predation data (K. Aydin, Alaska Fisheries Science Center, Seattle, WA, pers. comm.,
266 Table 3). For years where no data were available, an average rate over the 8 years was
267 used. The predation rate was calculated using the total numbers of walleye pollock
268 juveniles consumed by all groundfish predators in each year (Holsman and Aydin, 2015).
269 We computed mortality rates assuming that the maximum number consumed was
270 equivalent to a predation mortality rate of 0.3 per day (average). Predation rates for other
271 years were standardized relative to this maximum.
272
273 2.1.2.3 Movement of Juveniles

For vertical and horizontal movements of juveniles, new algorithms were incorporated into the original model of Hinckley et al. (1996). The vertical movement of juveniles is idealized, based on findings in Brodeur and Wilson (1996), who found that there is vertical migration in juvenile pollock. During the day, the distribution of juveniles is concentrated deeper in the water column, near 100 m or 30 m off the bottom, depending on water depth. During the night, distributions are higher in the water column, and more diffuse. Therefore, the migration algorithm added to this IBM is based on the time of day, where individuals are constrained to depth zones and within these depth zones, move up and down according to typical velocities of juveniles which are dependent on the length.

The vertical position of juveniles at each new time step, $Zj_{t+1}$(m), was calculated as in equation (1) where $Zj_t$ is depth at last time step, $w_j$ is the vertical mean velocity, and $\Delta t$ is the time step.

$$Zj_{t+1} = Zj_t + w_j \Delta t \qquad (1)$$

The mean magnitude of $w_j$ depended on juvenile length and was inferred from Hurst (2007). The mean magnitude of $w_j$ added to the deviance of $w_j$ was sampled randomly from a triangular distribution with mode, minimum ($0.05\, w_j$) and maximum value ($0.1\, w_j$) was used to obtain the position at each time step. The direction of $w_j$ (upward or downward) depended on a random deviate from a uniform distribution. The final depth in meters at each new time step was bounded with an upper and lower depth according to the hour (h) of the day in a 24 hour cycle (Equation 2 to 6).

| | | |
|---|---|---|
| h < 2 am | 40 m< $Zj_{t+1}$ < 60 m | (2) |
| 2 am< h < 5 am | 40 m< $Zj_{t+1}$ < 110m | (3) |
| 5 am< h < 2 pm | 90m < $Zj_{t+1}$ < 110m | (4) |
| 2 pm < h < 6 pm | 40m < $Zj_{t+1}$ < 110m | (5) |
| h > 6 pm | 40 m< $Zj_{t+1}$ < 60m | (6) |

When a particle is in an area of shallower water and the movement intervals are deeper than the bottom depth, then the particles are positioned 10 meters above the bottom plus a random deviation. Equations 2 and 6 show how pollock seek the euphotic zone during the night, presumably to reduce predation risk (Brodeur et al., 2000, Schabetsberger et al., 2003). Equation 4 is based on a vertical migratory behavior which assumes that juvenile pollock seek deeper depths during the day to avoid visual predation risk (Schabetsberger et al., 2003, Lang et al., 2000). A transition period of broader dispersion through the water column at dawn and dusk is set in equations 3 and 5.

Horizontally, the position of the juveniles was determined using a correlated random walk based on Kareiva and Shigesada (1983). We modeled movement paths as a sequence of straight lines in which juvenile displacement depended on size class. The position of the juvenile at each new time step, $Xj_{t+1}$ and $Yj_{t+1}$, depended on the position in the previous time step, $Xj_t$ and $Yj_t$ the length of the juvenile $Lj$, and the turning angle at the time step, $\alpha_{t+1}$. Turning angles were measured relative to the previous direction of movement according to the following equation,

$$\alpha_{t+1} = \alpha_t + \theta j \qquad (7)$$

where $\alpha_t$ was the turning angle at the previous time step, $\alpha_{t+1}$ was the turning angle at time $t + 1$ and $\theta j$ was chosen from a random normal probability distribution. Then, the new positions were,

$$Xj_{t+1} = Xj_t + Lj\cos(\alpha_{t+1}) \qquad (8)$$

$$Yj_{t+1} = Yj_t + Lj\sin(\alpha_{t+1}) \qquad (9)$$

2.1.2 The Hydrodynamic Model and Model Coupling

This modeling approach involved coupling the walleye pollock IBM to a circulation model, the Regional Ocean Modeling System (ROMS). ROMS is a free-surface, hydrostatic, primitive equation ocean circulation model that employs a nonlinear stretched vertical coordinate system that follows the bathymetry. The horizontal space is discretized using orthogonal curvilinear coordinates on an Arakawa C-grid (numerical

details can be found in Haidvogel et al. 2000, Shchepetkin and McWilliams, 2005). The ROMS simulations for this study used a 10 km (horizontal) grid (Northeast Pacific, NEP) with 42 vertical layers. A finer resolution version of the ROMS model (CGOA) on a 3 km grid has been developed since this exercise was done, however it was not available at the time. The NEP grid includes the GOA and the Bering Sea (BS). For this study, we used a subset of the output of a multi-decadal simulation of ROMS configured and run by Curchitser et al. (2005). Details of the physical model simulations and an assessment of the ROMS model's ability to reproduce observed modes of variability and their impact in the northeast Pacific can be found in Curchitser et al. (2005) and Parada et al. (This issue). The ROMS simulations were run with forcing scenarios (winds, freshwater and boundary conditions) appropriate for the year simulated. The hydrodynamic model produced daily averaged output consisting of salinity and temperature fields, 3D velocities and other variables. These were used to drive the IBM (offline) for 1987, the year used for this analysis.

A Java programming application (Ichthyop, Lett et al., 2008) was adapted to simulate the early life history of walleye pollock in the GOA. This application enabled us to calculate trajectories of particles representing individuals or groups of individual fish (superindividuals), and water properties (temperature, salinity) experienced by these particles during transport. The application used 3D fields of velocity, temperature, and salinity from simulations of ROMS to track particles within the model domain. The biological processes of the IBM are included as submodels within the modified Ichthyop application. The program stores information on the histories of individuals (e.g. time, longitude, latitude, depth, length, etc.). The Ichthyop application is distributed as a package that contains the program code and libraries. For this project, we used one of the early releases of the Ichthyops application and adapted it to our study requirements.

We used the Euler method as a particle tracking algorithm. We conducted a series of experiments comparing this method with the $4^{th}$ order Runge-Kutta method. The Runge-Kutta method was more stable than the Euler method, and converged quickly, however the Euler method did converge properly when enough iterations were used, and was much simpler and faster to run, and was therefore chosen for this study.

359 2.1.3 Survey Data and Model Simulations

360 A simulation experiment was run to examine the spatial and temporal matching
361 between modeled fields and observations of the distributions of successive life stages of
362 walleye pollock in the GOA for 1987 (1987 was the only year where there were multiple
363 surveys). The objective of the experiment was to use the coupled model to hindcast
364 distributions of larvae in May, early juveniles in June/July and later juveniles in
365 August/September for the year 1987, and to compare these model outputs to survey
366 distributions of young pollock for the periods 18-29 May, 1987, 18 June-16 July, 1987,
367 and 12 August-20 September, 1987. Model output from the date nearest the midpoint of
368 each survey was used to compare to survey data. A specific date was chosen to avoid
369 blurring of features that we wanted to be able to distinguish, such as patchiness and
370 current variability, blurring that would occur if we averaged over time. All tests were
371 done within the survey boundaries, except for the centroid analysis and the hotspot
372 analyses for the May time period. These analyses were done on both the very restricted
373 May survey area, and the broader modeled area, to compare the results for both areal
374 extents.

375 Methods for the May larval survey are described in Matarese et al. (2003). The
376 survey area was restricted to the region between Shelikof Strait Sutwik Island (Fig. 1).
377 The survey methods for the June/July and August/September cruises are covered in
378 Hinckley et al. (1991). The June/July survey for early juveniles covered much of the
379 western GOA on a regular grid, and used a Methot frame trawl (Methot 1986**).** The
380 August/September survey for late juveniles in 1987 made transects from Unimak Pass to
381 the eastern side of Kodiak Island, trawling with a 24-m high-opening shrimp trawl
382 (Hinckley et al. 1991).

383 Eggs in the model were released in 14 areas (5000 in each) identified as potential
384 spawning areas, on the 15$^{th}$ of each of 4 months (Feb, Mar, Apr, May), which covered the
385 bulk of the known spawning areas and times of pollock in the GOA (Kendall et al. 1996;
386 Matarese et al., 2003, Bailey et al., 2005, Doyle and Mier, This issue). The numbers of
387 eggs released was proportional to the egg production estimates from the stock
388 assessments for pollock, Dorn et al. 2005). The model was run using forcing for 1987,

through September. Individual locations and other information were recorded once every five days.

In order to focus the study only on the simulated individuals derived from spawning areas and times where fish caught in the surveys most likely originated, we obtained information on both spatial and temporal distribution of eggs (derived from the Alaska Fisheries Science Center (AFSC) Ichthyoplankton database, Matarese et al, 2003), and on hatchdate distributions of larvae and juveniles caught in the surveys in 1987, derived from otolith analysis (Brown and Bailey, 1992).

Figure 2 shows the pollock egg spatial distribution from ichthyoplankton surveys in 1987. It can be seen that the majority of eggs were found in North Shelikof Strait and the Shelikof Strait exit region. The highest number of eggs was caught in the first half of April (Fig. 3) and catches of eggs were near zero by the end of May. Hatchdates computed for larvae from the May survey and juveniles from the June/July and August/September surveys are presented in Brown and Bailey, 1992 (their Figure 5). This figure shows that hatchdates for all surveys were between the beginning of April and the end of May. These pieces of information indicated that we should only follow individual particles in the model that were released in April and May, in the North Shelikof Strait and the Shelikof Strait Exit areas.

### 2.1.4 Comparison Methods

Validation metrics included distributional centroids, their variance and directional ellipses, the Getis-Ord Gi* statistic (Ord and Getis, 1995), a normalized difference index (NDI), an overlap coefficient (OC) index, the Syrjala test statistics (Syrjala, 1996) and various other geostatistical spatial indices. Comparisons were made within the survey domain for all validation metrics with the exception of analyses for May, which were computed over the whole model domain as well as the survey region (a subset of the model domain). This was done due to the very small region surveyed in May.

Units for the surveys are densities (#/1000 $m^3$) for May and June/July. Units for the August/September survey were not normalized by area, but by time (# per 10 minutes tow). Units for the modeled “individuals” are “superindividual number”, which is the number of individual fish represented by each individual particle in the model. These

densities and numbers can be thought of as weighting factors for the spatial comparison methods, as they are not directly comparable, and in the case of the model, were not related to actual abundance of fish.

2.1.4.1 Distributional Centroids

We have calculated centroids (centers of gravity) for the model output and the survey data for each time period, May, June/July and August/September. Each centroid was calculated from the model output using latitude, longitude and superindividual number for each particle, and by using latitude, longitude and density of fish (catch per 1000 $m^3$ for May and June/July surveys, and catch per 10 min tow for the August/September survey) for the survey data. In the May case, centroids were calculated over the smaller survey area as well as the whole model domain for comparison purposes. Variances around these centroids (inertia) were also calculated. Directional ellipses and the related isotropy (the square root ratio between the minimal and the maximal inertia associated with the main directions of the ellipse) of one standard deviation from the mean were calculated and plotted to indicate the directional trend of the data. The centroids and directional ellipses of the model and the data were plotted to give a visual indication of how they compared. These statistics also formed part of the geostatistical comparison of spatial indices described below.

2.1.4.2 Hot/Coldspot Analysis

The Getis-Ord Gi* (Getis and Ord, 1992, Ord and Getis, 1995) is a technique used to examine spatial clustering of georeferenced data. The Getis-Ord Gi* statistic looks at each data point in the context of its neighbors. A data point with high values is only considered a statistically significant hotspot if it is surrounded by other points which also have high values, and the opposite for coldspots.

This statistic was calculated for each set of model output and survey data. Given a set of weighted points, this statistic identifies spatial clusters of high values (hotspots) and of low values (coldspots). The output of the analysis is Z scores and p-values for each feature, which represent the statistical significance of the spatial clustering of the values. Low or negative values of the Z score and low p-value indicate spatial clustering

of low values, and the opposite for high or positive Z scores. The higher (or lower) the Z score, the more intense the clustering. A Z score near zero indicates no apparent spatial clustering. A low p-value indicates a high (low) Z score is significantly different from zero, and hence the clustering of high (low) values is significant. This analysis was implemented in ArcView Version 10.

Prior to the following two analyses, the distributions of early (May cruise) larvae, early juveniles (June/July cruise) and late juveniles (August/September cruise) and model results were discretized in three bin sizes: 1/4° (~25 k), 1/2° (~50 k), and 3/4° (~75 k) spatial resolution. Then two methods were tested to account for model and data discrepancies: a normalized difference index and an overlap coefficient.

2.1.4.3 Normalized Difference Index (NDI)

A cost function was used to quantify the discrepancies between model and measurements, relating the difference to the variation of the measured variable. This was calculated by normalizing the difference between the mean field (by cell) from the model $\bar{Y}_{o,i}$ and observations $\bar{Y}_{m,i}$ respectively, with the standard deviation of observations by cell, following Berntsen et al. (1996) and Søiland and Skogen (2000). The cost function field $NDI_i$ for each $i$-th cell for the modeled and data fields is defined by:

$$NDI_i = (\bar{Y}_{o,i} - \bar{Y}_{m,i})/(sd\overline{(Y}_{o,i}) + 0.01) \quad (10)$$

The overall cost function NDI is the area average of the absolute values of the cost function field and was computed as the sum over all bins. NDI is always positive, while $NDI_i$ has both negative and positive values. The overall NDI was calculated for each bin size for the modeled and data fields for the May, June/July and August/September time periods. The overall smaller the overall NDI value the smaller the difference between model and data.

2.1.4.4 Overlap coefficient (OC)

This coefficient aims to estimate the spatial overlap between simulated and survey distributions of pollock and is based on Horn (1996) and Hinrichsen et al. (2005) studies. The overlap coefficient, OC, is 0 when no overlap is apparent and 1 when the two

distributions are identical (Hinrichsen et al., 2005). Hinrichsen et al (2005) applied this coefficient to determine how many larvae and prey were simultaneously present in the specified subareas of the central Baltic Sea (Hinrichsen et al., 2005). However, our application of OC is focused on model and data comparison and is defined by:

$$OC_i = 2\sum_{i=1}^{n_k}(x_i.\hat{x}_i)\,/(\sum_{i=1}^{n_k} x_i^2 + \sum_{i=1}^{n_k}\hat{x}_i^2) \quad (11)$$

Where $\hat{x}_i$ and $x_i$ are modeled and observed cell values respectively (for each individual bin $i$, and where $n_k$ is the number of bins in each of the three (k=1:3) bin sizes.

2.1.4.5 Syrjala Tests

Tests developed by Syrjala (1996) were applied to the model and survey distributions. Syrjala's test is a randomization test based on the Cramer von Mises statistic extended to bivariate distributions. These tests were developed to test the null hypothesis that there is no difference in the spatial distribution of two populations (here applied to the model and the survey distributions), versus the alternative hypothesis that the distributions are not the same. Two tests were applied: bivariate generalizations of 1) a Cramer-von Mises (CvM) type nonparametric test, and 2) a Kolmogirov-Smirnov (KS) type nonparametric test. For both tests, no specific distribution is assumed for either population. The data are normalized to the maximum densities for each distribution (model and data). These normalized values were then summed in 1/2° cells. The choice of cell size was based on balancing resolution with the number of cells occupied by modeled particles. The NDI and OC analyses showed that the 1/4° cells included very few particles, and the resolution of 3/4° was too coarse. The levels of abundance are not compared in these tests, just the spatial pattern. In these tests, the axes of the coordinate system describing the geographic locations which are being compared are rotated four times, once to each corner of the sampling grid, and an average of the test statistic for each rotation is calculated. This is to ameliorate the fact that the test statistic is not invariant with respect to the coordinate system used, although it does not vary by much (Syrjala, 1996). The significance of the test statistic is compared using a randomization test. Distributions were only compared for cells that were represented in both the surveys and the model output.

513 2.1.4.6 Geostatistical Simulation of Spatial Indices

514 A hypothesis testing procedure was also used to compare spatial distributions
515 observed during surveys to distributions from the model. The null hypothesis used in the
516 comparison was that 95% confidence intervals for the values of spatial indices derived
517 from the survey data contain the values of spatial indices from the IBM output.

518 To quantitatively describe walleye pollock spatial distributions, survey data and
519 model output (June/July and August/September only) were characterized using spatial
520 distribution indices developed by Woillez and colleagues (2007; 2009a). Spatial
521 distribution indices included: center of gravity (i.e. weighted location or centroid, as
522 above), inertia (variance of the spatial distribution), isotropy (evenness of dispersion),
523 positive area (the area occupied by densities > 0), spreading area (proportional area
524 occupied per unit area), and equivalent area (area occupied if all data cells had the same
525 density). Measures were compared within the survey region for all indices.

526 Confidence intervals for pollock spatial distribution indices derived from survey
527 data were calculated using geostatistical conditional simulations (Lantuéjoul, 2002). The
528 simulation of spatial distributions of young pollock was based on transformed Gaussian
529 simulations and on a Gibbs sampler to treat zero densities (Woillez, 2007; Woillez et al.,
530 2009b). The variogram of the Gaussian variable to be simulated was inferred using the
531 normal-scored, fish density variable, which included a concentration of values
532 corresponding to zero densities. Based on the inferred variogram model, Gibbs sampling
533 was used to simulate missing Gaussian values corresponding to these zeros, which were
534 lower than a threshold (determined from the proportion of zeros), and on the Gaussian
535 values of all other data points. The transformation was modeled as 0 below the threshold,
536 and by a linear interpolation above (corresponding to the non-zero values). This model
537 was also used at the end of the simulation to back-transform the Gaussian realizations to
538 raw data values. Multiple Gaussian realizations using observed or calculated Gaussian
539 values were produced and then back-transformed. Multiple realizations of pollock spatial
540 distributions were then used to compute spatial distribution index values. In this manner,
541 survey uncertainty was propagated to spatial indices and 95% empirical confidence
542 intervals were derived for each spatial index.

It is noteworthy that the support (i.e. set of locations with non-zero density values) helps define the resolution to be used for IBM simulations of pollock larvae and juvenile distributions. In this case the support is small, as the survey data are collected from vertical tows at station locations. First order distances from the survey data were computed, and the resolution of the simulation grid was set to 10 km, which was greater than the support and below that of the sampling lag. Variability in neighboring samples within cells (i.e. below resolution) was considered measurement error.

The hypothesis test consisted of determining whether the survey confidence intervals contained the value of the IBM distribution index. Three combinations of spawning release areas (cf. Fig. 1: area 8 – North Shelikof Strait; area 11 – Shelikof Strait exit region, or the two areas combined, and spawning months: April, May or the two months combined, were two factors tested to identify the combination of factors for each distribution index value that provided the best match between the IBM output and the survey data.

## 3.1 **Results**

### 3.1.1 General Features of Young Pollock Distributions

The survey area in May, 1987 was restricted to the area between Kodiak Island and Sutwik and Semidi Islands near the exit area of Shelikof Strait (Fig. 4). The distribution of early walleye pollock larvae in the May survey showed high densities east of Sutwik Islands and the Semidi Islands 130 km downstream of the observed spawning region in Shelikof Strait. The model output also showed a high density of early larvae in this area. An observed difference was that model showed a somewhat larger area of moderately high densities of early larvae in the broader region, to the northeast of the survey area in the exit region of Shelikof Strait, and to the southwest of the survey region, in areas which were not covered by the survey. We have no way of knowing whether pollock larvae would have been found in these regions outside the survey area. Note however, that centroids of pollock distribution from the model output and data centroids are in close proximity, near Sutwik Island, even given the larger model domain. This supports the choice of the survey area as being the center of the pollock larval distribution at this time.

The distribution of early juvenile walleye pollock in June/July in the survey data showed maximum densities between the Sutwik/Semidi Islands and the Shumagin Islands (Fig. 5). The model showed high density peaks located in the same area during the same time period. It can be seen in Figure 5 that the centroids of distribution are downstream of those seen in May for both the survey data and the modeled individuals (the Alaska Coastal Current flows through Shelikof Strait from northeast to southwest) as described by Hinckley et al (1991), and that all centroids were clustered near the Shumagin Islands in close proximity to each other. The centroid for the survey was a slightly to the east, however, compared to the model.

The modeled distribution of later 0-age juvenile walleye pollock in August/September was located around the Shumagin Islands (Fig. 6). The highest densities of modeled individuals were somewhat to the east and inshore of the Shumagins. The survey data also showed maximum densities near the Shumagins (Fig 6). In the survey some juveniles were also found around Kodiak Island, which the model did not show, probably because individuals spawned outside Shelikof Strait were excluded. The survey did not cover the Bering Sea, however, the model showed juveniles transiting to this region (see Parada et al., This issue). The centroids of the modeled distributions (excluding the fish that transited to the Bering Sea) and the survey distributions were both located in the area to the inside of the Shumagin Islands, near to the Alaska Peninsula.

Figure 7 shows directional ellipses of one standard deviation from the mean locations and are plotted to indicate the directional trend of the data. The figure indicates that the directional trend of the survey and the model results were similar, both were oriented in the northeast/southwest directions. This is the main direction of currents in this area, although current strength in the region between Sutwik Island and the Shumagin Islands is not strong and can be somewhat variable in direction. The larger size of the model ellipses in May represents the fact that the survey area was much smaller than the modeled area. The relative size of the ellipses in June/July for model and data were similar. The survey data ellipse was larger in August/September because, although the regions compared were the same (ie. model and data were only compared within the survey area boundaries), the survey found juvenile pollock around Kodiak that were not present in the model output for reasons we will consider in the Discussion.

605
606 3.1.2 Hot/Coldspot Analysis
607 The Getis-Ord Gi* statistic showed distinct hot and coldspots within the May
608 survey distributions, indicating that the distribution was quite heterogeneous even within
609 this small survey region (Fig. 8). Locations with high densities (hotspots) were located in
610 the northern part of the survey area, whereas locations with lower densities (coldspots)
611 were more often found in the southern part of the distribution. The modeled distribution
612 for May, on the other hand, showed no distinct hot or coldspots, with the exception of
613 some weak hotspots just to the east of the Shumagin Islands, which was, of course,
614 outside the May survey area. There were also no evident hot or coldspots in the modeled
615 distribution when it was examined within the survey area
616 The June/July survey distribution showed distinct clusters of hotspots (Fig. 9),
617 mostly located between Sutwik I. and the Shumagin Islands, near the coast of the Alaska
618 Peninsula. The modeled distribution for this time period showed a few weak hotspots in
619 this region, however several hotspots were also seen to the west of the Shumagins.
620 Notable in the June/July modeled distribution was a large cluster of particles with low
621 superindividual counts (coldspot) nearshore of the Shumagin Islands (seen in blue on Fig.
622 9). The data showed high catches in this region. An analysis of the particles found in
623 this model coldspot showed that 58% were spawned in April, with the rest spawned in
624 May. Also, 66% were spawned in the Shelikof Exit region, rather than North Shelikof
625 Strait.
626 This analysis for the August/September time period shows more agreement
627 between the model and the survey results. The August/September survey distribution
628 showed hotspots in several regions: near the coast just to the west of Sutwik Island, and
629 to the west of the Shumagin Islands (Fig. 10). The modeled distribution for this time
630 period also showed several hotspots to the west and offshore of the Shumagin Islands, as
631 well as the intense coldspot in the same location (nearshore of the Shumagin Islands) as
632 in the June/July model output. Of the particles/individuals found in the coldspot area in
633 August/September, 66% were spawned in May, and 63% came from the Shelikof exit
634 region.
635

636 3.1.3 Normalized Difference Index

637 The cost function $NDI_i$ field (Figure 11) was calculated for each bin size (columns
638 in the figure) for the modeled and data fields for the three time periods (rows in the
639 figure). Model and data were compared within the survey area for each time period.
640 The overall NDI for the May time period showed minimum differences (132.4) at a bin
641 size of 3/4° and a maximum NDI at a bin size of 1/4° (3245.5). The $NDI_i$ fields showed
642 positive differences (observed values greater than the model) in several cells near Sutwik
643 and the Semidi Islands (Fig. 1). At the 1/4° bin size during May, differences were seen in
644 several cells on the northeast border of the survey area. Little difference between model
645 and observations were seen for May at the 3/4° bin size. The overall NDI for the
646 June/July time period again showed a maximum value at a bin size of 1/4° (7903.8), and
647 a minimum NDI at a bin size of 3/4° (835.1). During this time period, positive
648 differences in $NDI_i$ (observed values greater than the model) were seen using the 1/4°
649 and 1/2° bins at several scattered locations between Kodiak Island and the Shumagins,
650 however the $NDI_i$ fields were spatially quite uniform at the 3/4° bin sizes with only
651 minor positive differences between model and data.

652 During the August/September time period, the overall NDI showed a large
653 maximum (8843.0) at the 1/4° bin size, and a minimum at the 3/4° bin size (1620.5). At
654 the smallest bin size, positive $NDI_i$ values were seen in a cell near Sutwik Island, with
655 several more just to the west of the Shumagin Islands. A positive $NDI_i$ was seen near
656 Sutwik also in the 1/2° bin at this time period, and also in several cells to the northeast of
657 Kodiak Island and to the west of the Shumagins. At the 3/4° bin size during this period,
658 differences were seen just offshore of the Shumagin Islands, and to the northeast of
659 Kodiak Island, however there were more cells with no difference between model and
660 data. Overall, the differences between model and data were always positive, ie. the
661 observed values were greater than the model. The differences between model and data
662 were smallest at the largest bin size. During the June/July period, large areas showed no
663 differences between the model and data.

664

665 3.1.4 Overlap coefficient:

The OC estimates the spatial overlap between simulated and data distributions, with higher values indicating more overlap. In May, the overall OC was the smallest at the smallest bin size, and largest at the largest bin size. At all three bin sizes, the $OC_i$s in May were highest near Sutwik Island. The local OC in May was highest at a bin size of 1/4° with values of 0.4 to 0.8, while the local OCs at bin sizes of 1/2° and 3/4° were on the order of 0.3 and 0.1 respectively (Fig.12). During the June/July time period, the overall OC showed the highest value (0.2) seen at the 1/4° bin size, and the lowest OC (0.07) at the 1/2° bin size. Bins with higher local $OC_i$ during June/July were seen around and to the east of the Shumagin Islands at all three bin sizes. During the August/September time period, the overall OC was the same (0.2) at the smallest and largest bin sizes, with smaller OC seen using the 1/2° bin size (0.1). At all three bin sizes, the highest local $OC_i$ values were seen around the Shumagin Islands and somewhat to the west. In general the highest overlap between the model and data occurred during the June/July survey.

3.1.5 Syrjala Tests

Both of the Syrjala test statistics for the May distributions showed no significant difference between the modeled and survey distributions at $p = 0.05$ (Table 4). The power of this test was relatively low, as only there were only 13 cells in common between the model and the survey (as the survey area represented a very small portion of the total area occupied by the modeled distribution). The Syrjala test statistics on the June/July distributions were different at the $p = 0.05$ level. Neither test showed the August/September model and survey distributions to be significantly different.

3.1.6 Geostatistical Simulation of Spatial Indices

For both surveys (June/July and August/September), pollock density was highly skewed. A high (37.5%) proportion of zeros was observed in the 1987 June/July survey. In contrast, there were no zeros observed in the 1987 August/September survey, but there were low values in the data. To apply the simulation method to estimate confidence intervals (Woillez, et al. 2009b) for both surveys, values below a density of 17 per 10 min

696 sample were considered zero values. The thresholded zero values represented 18.9% of
697 the 1987 August/September survey data.
698 The first step when calculating confidence intervals around the survey data was
699 the normal-score transformation of fish densities. As shown in Figure 13 a,b, this
700 transformation was 0 below the threshold value of 17 per 10 min sample, and linearly
701 interpolated above that threshold. As the Gaussian variable to be simulated was not
702 known at all locations, the variogram model of the Gaussian variable was indirectly fit
703 using the variogram of the normal-scored variable (Woillez, 2007). The variogram model
704 of the Gaussian variable was a nested structure with a nugget of 0.25, a Gaussian
705 component of 0.45 with a range of 150 kilometers, and a spherical component of 0.80
706 with a range of 600 kilometers for the 1987 June/July survey (Fig. 13c). A nested
707 structure with a nugget of 0.4, a spherical component of 0.6 with a range of 175
708 kilometers was the variogram model used for the 1987 August/September survey (Fig.
709 13d).
710 Gibbs sampling was used to simulate Gaussian values at locations corresponding
711 to zeros. Then, a classical conditional simulation (i.e. a geostatistical simulation
712 incorporating known data values) was performed to generate multiple realizations of the
713 Gaussian variable, which were transformed to pollock densities values (Fig. 14). A total
714 of 250 realizations of pollock spatial distributions were simulated over a 10 km x 10 km
715 grid for the 1987 June/July (Fig. 14 a,b,c) and August/September (Fig. 14 d,e,f) survey
716 areas. Highest pollock average densities were concentrated between the Semidi and
717 Shumagin Island groups during June and July, as indicated by the center of gravity and
718 inertia axes, shifting and extending southwest from the Shumagin Islands to Unalaska
719 Island in the later survey.
720 Spatial distribution index values and 95% confidence intervals for survey data and
721 IBM outputs are summarized in Table 5. For the June/July survey, all spatial indices
722 computed from the survey data are contained within the confidence intervals generated
723 by geostatistical conditional simulations from the survey data. The occurrence of index
724 values calculated from model output occurring within confidence intervals depended on
725 area and month. For the August/September survey, all spatial indices except inertia were
726 contained within the confidence intervals. Inertia from 97.5% of the IBM simulated fields

727 was higher than inertia index values computed from the survey data, and therefore this
728 index wasn't used for the comparison between the survey data and the individual based
729 model.
730 For both survey periods, the latitude of the center of gravity (i.e. ycg) was the
731 model index most often included within the confidence intervals (Table 5) from the
732 survey data, occurring within the confidence intervals for the June/July survey when
733 particles were released in April area 11 (Shelikof Strait Exit region), and 8 (Shelikof
734 Strait North) and 11 combined. For particles released in May or when April and May
735 releases were combined, the latitudinal component of the center of gravity occurred
736 within confidence intervals in both release areas. For the August/September survey, the
737 latitude component of the center of gravity occurred inside the confidence intervals
738 regardless of where particles were released in April, and in area 8 for both release months
739 (Table 5). The longitude of the center of gravity only occurred inside the confidence
740 interval in the June/July survey when particles were released in April, and in area 8 for
741 both release months (Table 5). The isotropy metric was contained within the confidence
742 intervals when particles were released in April in area 8 for the period June/July, and in
743 April in area 11 and 8 & 11 for the period August/September (Table 5). Inertia was
744 included only in the August/September confidence interval when particles were released
745 in May and area 11, however this case is not meaningful as the inertia from the survey
746 data was not contained in the confidence interval. Finally, none of the occupation area
747 indices were included in the confidence intervals. The IBM produced spatial distributions
748 which always occupied smaller areas than those from the surveys.
749 To conclude this comparison, two (center of gravity and isotropy) of six spatial
750 indices (inertia excluded) are included within survey data confidence intervals for each
751 period independently or jointly. Particles from the IBM released in April in the Shelikof
752 Strait exit region (Area 11) or when combined with the North Shelikof region (Area 8)
753 produced spatial distributions that best matched spatial distributions from the two
754 surveys. For the June/July survey data, the longitude and the latitude of the center of
755 gravity were reproduced by the IBM output-derived indices. The latitude of the center of
756 gravity and the isotropy indices from the IBM output data matched those in the
757 August/September survey data.

758

759 4.1 **Discussion**

760 We used several methods to visualize the difference between the model output and the
761 survey data (methods summarized in Table 6, results summarized in Table 7). All of the
762 methods applied in this study were useful in different ways. The plotting of centroids and
763 their variance and isotropy enables visualization of similarities and differences in overall
764 observed and predicted spatial distributions. The Getis-Ord Gi* statistic provides an
765 index of spatial patchiness. The NDI and OC identified differences and overlaps between
766 the model output and the survey data, both globally and locally, and the NDI had the
767 added advantage of indicating whether model values were higher than the data or the
768 opposite, as well as where the differences were located. The Syrjala statistics provide a
769 statistical comparison of the two distributions, and were easy to apply, however they are
770 not informative about the details of the distributions that cause agreement or differences.
771 Despite its complexity of implementation, the geostatistical spatial indices comparison
772 has the added advantage of identifying specific characteristics of survey spatial
773 distributions that are reproduced by the IBM model. If the objective is to use IBMs to
774 reproduce observed spatial distributions, then the extent of match or mismatch in
775 geostatistical spatial indices can be used to identify properties of the IBM for refinement.
776 Visual inspection of the distributions, the centroids and their variance and
777 directional ellipses, showed that the modeled distribution was consistent with the
778 geostatistical comparison of spatial indices. These measures showed reasonable good fit
779 between model and data. Centroid analysis has been used to compare spatial distributions
780 (Alvares et al., 2000, Castaño-Primo et al., 2014, Ernst et al., 2005; Vikebø et al. 2005),
781 even though one of the drawbacks of this approach is that it is a global statistic that does
782 not tell you about local aggregations. This type of visual comparison can be a good first
783 step in a model validation exercise. Although global indicators of spatial association
784 indicate whether mapped data exhibits an organized pattern, care must be taken in
785 interpreting the results. A global trend of spatial autocorrelation may mask the
786 magnitude and direction of spatial heterogeneity.
787 The Getis-Ord Gi* statistic, or hot/coldspot analysis (Getis and Ord, 1992, Ord
788 and Getis, 1995) quantifies patchiness of the distributions. This statistic gives the sum of

789 attribute values in a given region and the surrounding regions within a distance band
790 relative to the sum of all values of the considered variable. Significant deviations of the
791 Getis-Ord Gi* values from the expected value indicate local clustering. If the deviation
792 is significantly positive, the spatial cluster is called a hotspot (Kosfeld and Lauridsen,
793 2012). Care must be taken in deciding upon the size of the neighborhood (the distance
794 band), as patterns may change with different size bands. The results of this analysis were
795 not consistent between model and data, probably due to the heterogeneity of currents in
796 this area.
797 The Normalized Difference Index (NDI) and the Overlap Coefficient (OC)
798 methodologies seem to be complementary, providing information in terms of the overlap
799 between model and data, and the level of discrepancies between quantities assessed.
800 However, the NDI and the OC analyses require binning survey data and the model
801 information at a common resolution. The challenge is to determine an appropriate
802 resolution that represents the information obtained from the model and the survey data.
803 This is the "binning problem" that arises when comparing spatial model output and
804 empirical data. In geography, this challenge is related to the modifiable areal unit
805 problem (MAUP) arising from the imposition of artificial units of spatial reporting on
806 continuous geographical phenomena, which may generate artificial spatial patterns
807 (Heywood, 1988). When using these indices on output derived from a Lagrangian model,
808 it is also important to consider that at the smallest bin size there will be a lower level of
809 co-occurrence between survey stations and the occurrence of modelled particles. A
810 balance must be found between resolution and the number of occupied cells. The
811 binning problem and the selection of a given bin size may affect the outcomes of the
812 analysis. Sensitivity analyses may be needed in order to make this choice. In the case of
813 the model output, the hydrodynamics model resolution will be indicative of the lowest
814 limit of the bin size, while the upper level is definition is less clear. These two indices
815 showed local areas of differences which did vary with bin size. The smallest differences
816 and highest overlap were seen during the June/July time period.
817 Syrjala's statistics were used to analyze the spatial difference between predicted
818 and observed distributions of young pollock. Results from the Syrjala tests showed
819 agreement between the modeled and survey distributions for two of the three time

820 periods. The KS statistic used in the Syrjala tests measures the greatest difference
821 between the two cumulative distributions. It is therefore sensitive to small numbers of
822 extreme values in the distributions (Syrjala, 1996). Extreme values can be a difficulty,
823 although this did not appear to be an issue with our datasets, as the results for both
824 statistics were the same. As noted by Syrjala, fish may be patchily distributed (due to
825 concentration by currents, behavior, etc), yet fundamentally similar in overall
826 distribution. The Syrjala tests (Syrjala, 1996) provided a statistical means to test the
827 difference between the modeled versus survey distributions, that is very easy to
828 implement, as it has been coded into the R language (in the Ecespa package). However,
829 this test is a global analysis while the Getis-Ord Gi* analysis provide information in
830 terms of local clustering.
831 Geostatistical simulation was used to derive confidence intervals for all spatial
832 indices calculated using the survey data. Accuracy of the confidence intervals depends on
833 the appropriate implementation of the geostatistical simulation used to evaluate survey
834 uncertainty. Different approaches exist for validating geostatistical simulations. Each of
835 these approaches is appropriate for a different component of the simulation: the stochastic
836 model, the spatial domain, and the simulation algorithm. For instance, a cross-validation
837 exercise can be performed to check the accuracy of the simulation against a set of
838 empirical data (Deutsch, 1997) to evaluate the simulation algorithm and the stochastic
839 model. Statistical tests also exist for validating the simulation algorithm (Emery, 2008).
840 These methods check whether the mean value, the dispersion variance, or the variogram
841 are reproduced, and indicate whether observed fluctuations in output values are consistent
842 with the random field model and with the size of the domain where simulation is
843 performed. In our simulation, the mean value was tested, the variogram was visually
844 checked, and the multivariate distributions (i.e. the two first moments) of the simulated
845 random field were compared to those of the model.
846 The comparison of spatial indices showed that the center of gravity (centroid) and
847 to a lesser extent, isotropy (for specific release dates and areas), were the indices that
848 were the most similar for the IBM and the survey data. Inertia, isotropy and measures of
849 spatial coverage might not be expected to compare well in a region such as the GOA.
850 The currents in this region are complex, and the hydrodynamic model cannot replicate

this complexity to a high degree of accuracy, even though aggregate statistical comparisons of the modeled and observed currents do well. Since the larvae follow the currents for much of their early life, and these currents differ in detail from the real world, details of the distributions of particles would not be expected to do as well as aggregate measures such as centroids.

The purpose of the IBM was to generate realistic distributions and survival of young pollock over time. Spatial distributions produced from the two survey data sets analyzed in the geostatistical part of our study were treated as spatial point processes, where density or number weights were attributed to each point (i.e. the concept of superindividuals). Therefore, the predicted spatial distributions can only be considered as approximations of the true underlying spatial distribution. A potential modification to improve matches between survey data and model predictions would be to propagate the uncertainty of model-predicted spatial distributions to the IBM-based spatial indices. Then, the comparison of spatial distributions between IBM and survey could be based on the overlap between survey and model spatial index confidence intervals. Such uncertainty in model-based spatial distributions may be one reason why occupation area indices of the survey-model comparison performed poorly.

Differences in spatial distributions between IBM model output and data from surveys may be attributed to several factors. There may be differences between survey and model initial conditions (ie. the location and timing of spawning by fish caught in the survey compared to the initial distribution of particle releases in the model simulation). We addressed this possibility as best we could by examining only individuals released at times and locations of most of the known spawning for 1987 (Kendall et al. 1996). There may have been fish caught in the surveys that were spawned in other locations at other times, however only small amounts of spawning have been observed in other locations (Wilson, 2000). For example, it is thought that juvenile pollock found around Kodiak Island probably originated from spawning in areas around Kodiak other than Shelikof Strait (Bailey et al., 1999, Wilson, 2000). Since we only examined model output from individuals released in Shelikof Strait, these Kodiak fish would have been excluded. This issue may have influenced the mismatch of area-occupied indices between empirical and modeled data.

882 Differences between survey and model estimates may also be a result of using
883 locally random initial conditions for this model simulation in spite of choosing
884 individuals from specific areas and times. Individuals were released randomly within the
885 North Shelikof and Shelikof Exit zones once per month. Pollock spawning occurs
886 continuously in very dense aggregations in Shelikof Strait; spawning is highly localized
887 both in time and space, and is concentrated near line 8 (Fig. 1) in the first two weeks of
888 April (Kendall, et al. 1996).
889 Differences between model output and survey data could also be related to the
890 limitations of the hydrodynamic model. The ROMs output used in these simulation had a
891 relatively coarse resolution in the coastal regions of 10 km compared with more recent
892 configurations of ROMS, such as the 3 km resolution model now in use (Dobbins et al.
893 2009, Coyle et al. 2012). Physical processes with a higher spatial resolution are not
894 resolved by simulations with the 10 km model. Also, bottom topography is smoothed
895 significantly in some regions in the 10 km model. This has implications for flow patterns.
896 Divergence between the real and the modeled flow fields is a common problem for all
897 numerical ocean models due to small and mesoscale factors such as eddies, meanders,
898 and the chaotic behavior of the real fields, which the models cannot replicate. This can
899 be adjusted for if enough data exist which can be assimilated to correct the flow fields.
900 This was not possible in our case due to the paucity of available data.
901 Another model condition that may result in different empirical and model-
902 predicted juvenile fish distributions are the movement algorithms and the resulting
903 interactions with the flow field (Hinckley et al. 1996, Werner et al. 1996, 2001,
904 Hinrichsen et al. 2002, Fox et al. 2006, Staaterman and Paris, 2014). The vertical and
905 horizontal movements of fish are affected by their life stage (Clark et al. 2005), and thus
906 by their size, which in turn is affected by several factors from temperature to
907 consumption rates. Inevitably, it is not possible, nor is it the goal, to replicate these
908 patterns exactly in the models. The horizontal movement submodel incorporated for
909 older juvenile pollock in this IBM is based on a correlated random walk (CRW). Since
910 most animals have a tendency to move in a forward direction, CRWs have been used to
911 model animal paths (Siniff and Jessen 1969, Skellam 1973, Kareiva and Shigesada 1983,
912 Bovet and Benhamou 1988, Turchin 1998, Willis, 2011). As a caution, Codling et al.

913 (2008) describe how CRWs can produce a local directional bias in which each step tends
914 to point in the same direction as the previous one, although the influence of the initial
915 direction of motion progressively diminishes over time, and step orientations are
916 uniformly distributed in the long term (Benhamou 2006). The algorithm implemented in
917 this model seemed to produce distributions of older juveniles which agreed with data
918 relatively well, in terms of several measures used (Table 7). However, distributions of
919 juveniles which are more active later in the year may require refinements in the
920 swimming algorithm, ie. consideration of factors such as more realistic modeling of
921 directionality of swimming, such as movement towards food (Huebert and Sponaugle,
922 2009, see Staaterman and Paris, 2014 for a review).
923 The model presents some interesting results concerning the early life history of
924 pollock in this region. For example, the concentration of modeled particles near the coast
925 of the Alaska Peninsula, inshore of the Shumagin Islands, as shown by the Getis-Ord Gi*
926 statistic indicates that this may be a collection area for fish/particles. This result
927 corresponds to observations that high densities of juveniles are found in this region
928 (Hinckley et al. 1991, Brodeur et al., 1995, Wilson et al. 1996, our data). Also, the
929 percentages of modeled particles found which had low superindividual numbers in
930 June/July that were spawned in April indicates that the individuals had been in the water
931 longer than those spawned in May and had therefore been exposed to higher mortality
932 than those found elsewhere. This pattern was reversed in the August/September period,
933 with more particles in this region having been released in May rather than April. This
934 may reflect the addition of particles with time to this area. The majority of particles in the
935 coldspot area were released in the Shelikof Strait Exit region rather than the more distant
936 North Shelikof Strait, thus the trajectories of these individuals to the coldspot region were
937 either less direct, or the individuals had remained in the coldspot area longer. The fact
938 that this coldspot was present in both the June/July and the August/September time
939 period indicates that the latter is more likely. The model indicates that this region near
940 the Shumagin Islands concentrates juvenile fish and may function as a productive nursery
941 area.
942 The walleye pollock model correctly predicted that the Shumagin Island area,
943 especially the nearshore areas, is an important nursery area, and also that the origin of

944 many of the Shumagin Island juveniles is most likely to have been eggs spawned in
945 Shelikof Strait in April. This is consistent with the idea of the Shelikof-Shumagin
946 spawning-nursery area pair (Hinckley et al., 1991). There is also evidence that the area
947 near Sutwik Island may play a role as potential nursery areas (Mazur et al., 2007), which
948 is consistent with the model predictions.
949 In conclusion, we recommend a multistep process for the validation of spatial
950 output of biophysical IBMs, starting with visual comparisons and simple descriptive
951 statistics, then calculation of indices showing features of interest, and finally, using
952 hypothesis testing statistical and geostatistical approaches that can give measures of
953 statistical significance to the differences/similarity between spatial model output and
954 data. Model validation and model improvement is an iterative process where
955 mismatches between model and data can be used to improve the model and the surveys
956 (if they can be specifically designed to compare with model output). However, for some
957 purposes such as management applications, "success" in validation must be defined.
958 Some methods, such as visual inspections, the NDI and the OC require the user to define
959 "success" in matching model and data, as this can be dependent on bin size. A new
960 convention is needed to delineate success thresholds, perhaps from sensitivity analyses,
961 for the validation process of biophysical IBMs.
962
963 **Acknowledgements**
964 We thank the North Pacific Research Board for funding Project 523: Pollock
965 recruitment and stock structure, which supported portions of this research. Dr. A.J.
966 Hermann developed the ROMS model for the Gulf of Alaska which drives the pollock
967 IBM. We would also like to acknowledge support from the EcoFOCI group and the
968 RACE Division at the Alaska Fisheries Science Center, which provided data, personnel
969 salaries, and other support. The findings and conclusions in the paper are those of the
970 authors and do not necessarily represent the views of the National Marine Fisheries
971 Service.
972
973
974

**References**


Alvera-Azcarate, A., Barth, A., Bouallegue, Z.B., Rixen, M., Beckers, J.M. 2007. Forecast verification of a 3D model of the Mediterranean Sea. The use of discrete wavelet transforms and EOFs in the skill assessment of spatial forecasts. J. Mar. Syst. 65: 460-483.

Alvarez, P., Motos, L., Uriarte, A., Egana, J. 2001. Spatial and temporal distribution of European hake, *Merluccius merluccius* (L.), eggs and larvae in relation to hydrographical conditions in the Bay of Biscay. Fish. Research 50: 111-128

Bailey, K.M., Bond, N.A., Stabeno, P.J., 1999. Anomalous transport of walleye pollock larvae linked to ocean and atmospheric patterns in May 1996. Fish. Oceanogr. 8: 264-273.

Bailey, K.M., L. Ciannelli, N.A. Bond, A. Belgrano, and N.C. Stenseth. 2005. Recruitment of walleye pollock in a physically and biologically complex ecosystem: A new perspective. Prog. Oceanogr. 67: 24-42.

Bartsch, J., and Coombs, S. 2004. An individual-based model of the early life history of mackerel (*Scomber scombrus*) in the eastern North Atlantic, simulating transport, growth, and mortality. Fish. Oceanogr, 13: 365–379.

Beck, M.W., Heck, K.L., Able, Jr. K.W., Childers, D.L., Eggleston, D.B., Gillanders, B.M., Halpern, B., Hays, C.G., Hoshino, H., Minello, T.J., Orth, R.J., Sheridan, P.F., Weinstein, M.P., 2001. The identification, conservation, and management of

1005 estuarine and marine nurseries for fish and invertebrates. BioScience. 51: 633-
1006 641.
1007 Becker, B.J., Levin, L.A., Fodrie, F., McMillan, P.A. 2007. Complex larval connectivity
1008 patterns among marine invertebrate populations. Proc. Nat. Acad. Sci. 104: 3267-
1009 3272.
1010 Benhamou, S. 2006. Detecting an orientation component in animal paths when the
1011 preferred direction is individual-dependent. Ecology 87: 518-528.
1012 Berntsen, J., Svendsen, E., and Ostrowski, M. 1996. Validation and sensitivity study of a
1013 sigma-coordinate ocean model using SKAGEX dataset. ICES CM 1996/C:5.
1014 Bevelhimer, M.S., and Adams, S.M. 1993. A bioenergetic analysis of diel vertical
1015 migration by kokanee salmon, *Oncorhynchus nerka*. Can. J. Fish. Aquat. Sci. **50**:
1016 2336-2349.
1017 Bez, N. 2000. On the use of Lloyd's index of patchiness. Fish. Oceanogr. 9(4): 372-
1018 376.
1019 Blood D.M., Matarese, A.C., Yoklavich, M.M., 1994. Embryonic development of
1020 walleye pollock *Theragra chalcogramma*, from Shelikof Strait, Gulf of Alaska.
1021 Fish. Bull. US 92, 207-222.
1022 Bovet, P. and Benhamou, S. 1988 Spatial analysis of animals' movements using a
1023 correlated random walk model. J. Theor. Biol. 131: 419 – 433.
1024 (doi:10.1016/S0022-5193(88)80038-9).
1025 Brodeur, R. D., M. S. Busby, and M. T. Wilson. 1995. Summer distribution of early life
1026 stages of walleye pollock,*Theragra chalcogramma,* and associated species in the
1027 western Gulf of Alaska. Fish. Bull. 93: 603-618.
1028 Brodeur, R.D. and Wilson, M.T. 1996. Mesoscale acoustic patterns of juvenile walleye
1029 pollock (*Theragra chalcogramma*) in the western Gulf of Alaska. Can. J. Fish.
1030 Aquat. Sci. 53: 1951-1963.
1031 Brodeur, R. D., Wilson, M.T., Ciannelli, L. 2000. Spatial and temporal variability in
1032 feeding and condition of age-0 walleye pollock (*Theragra chalcogramma*) in
1033 frontal regions of the Bering Sea. ICES J. Mar. Sci. 57: 256–264.
1034 Brown, A.L., and Bailey, K.M. 1992. Otolith analysis of juvenile pollock *Theragra*
1035 *chalcogramma* from the western Gulf of Alaska. Mar. Biol. 112: 23-30.

1036 Campana, S.E. 1999. Chemistry and composition of fish otoliths: pathways, mechanisms
1037 and applications. Mar. Ecol. Prog. Ser. 188: 263-297.
1038 Castaño-Primo, R., Vikebø, F. B., and Sundby,S. 2014. A model approach to identify
1039 the spawning grounds and describing the early life history of Northeast Arctic
1040 haddock (*Melanogrammus aeglefinus*). ICES J. of Mar. Sci. 71(9): 2505–2514.
1041 Ciannelli, L., Brodeur, R.D., Buckley, T.W., 1998. Development and application of a
1042 bioenergetics model for juvenile walleye pollock. J. Fish Biol. 52: 879–898.
1043 Clark DL, Leis JM, Hay AC, Trnski T (2005) Swimming ontogeny of larvae of four
1044 temperate marine fishes. Mar Ecol Prog Ser 292: 287–300.
1045 Codling, E.A., Plank, M.J., Benhamou, S. 2008. Random walk models in biology. J. R.
1046 Soc. Interface 2008 5, doi: 10.1098/rsif.2008.0014,
1047 Coscia, I., Robins, P.E., Porter, J.S., Malham, S.K., Ironside, J.E. 2013. Modelled larval
1048 dispersal and measured gene flow: seascape genetics of the common cockle
1049 *Cerastoderma edule* in the southern Irish Sea. Conservation Genetics 14: 451-
1050 466.
1051 Cotter, A. J. R., Burt, L., Paxton, C. G. M., Fernandez, C., Buckland, S. T., and Pan, J-X.
1052 2004. Are stock assessment methods too complicated? Fish and Fisheries, 5: 235
1053 – 254.
1054 Coyle, K., Cheng, W., S.L. Hinckley, E.J. Lessard, T. Whitledge, A.J. Hermann and K.
1055 Hedstrom. 2012. Model and field observations of effects of circulation on the
1056 timing and magnitude of nitrate utilization and production on the northern Gulf of
1057 Alaska shelf. Progress in Oceanography, 103:16-41,
1058 doi:10.1016/j.pocean.2012.03.002.
1059 Curchitser, E.N., Haidvogel, D.B., Hermann, A.J., Dobbins, E.L., Powell, T., Kaplan, A.,
1060 2005. Multi-scale modeling of the North Pacific Ocean: Assessment of simulated
1061 basin-scale variability (1996-2003). J. Geophys. Res. 110, C11021,
1062 doi:101029/2005JC002902.
1063 Deegan, L.A., 1993. Nutrient and energy transport between estuaries and coastal marine
1064 ecosystems by fish migration. Can. J. Fish. Aquat. Sci. 50, 74-79.

1065 Delhez, E.J.M., Damm,P., de Goede, E., de Kok, J.M., Dumas, F., Gerritsen, H., Jones, J.
1066 E., *et al.* 2004. Variability of shelf-seas hydrodynamic models: lessons from the
1067 NOMADS2 Project. J. of Mar. Systems, 45: 39–53.
1068 Deutsch, C.V., 1997. Direct assessment of local accuracy and precision. In: Baafi, E.Y.,
1069 Schofield, N.A. (Eds.), Geostatistics Wollongong '96. Kluwer Academic,
1070 Dordrecht, pp. 115–125.
1071 De Robertis, A., Schell, C., Jaffe, J.S. 2003. Acoustic observations of the swimming
1072 behavior of the euphausiid *Euphausia pacifica* Hansen ICES J. Mar. Sci. 60 (4):
1073 885-898 doi:10.1016/S1054-3139(03)00070-5
1074 DiBacco, C., and Levin, L.A. 2000. Development and application of elemental
1075 fingerprinting to track the dispersal of marine invertebrate larvae. Limnology and
1076 Oceanography 45: 871-880.
1077 Dobbins, E.L., Hermann, A.J., Stabeno, P.J., Bond, N.A., Steed, R.C. 2009. Modeled
1078 transport of freshwater from a line-source in the coastal Gulf of Alaska. Deep Sea
1079 Research II, doi:10.1016/j.dsr2.2009.02.004
1080 Dorn. M., Aydin, K., Barbeaux, S., Guttormsen, M., Megrey, B., Spalinger, K., Wilkins,
1081 M., 2005. Assessment of walleye pollock in the Gulf of Alaska In: Appendix B.
1082 Stock assessment and fishery evaluation report for the Groundfish Resources of
1083 the Gulf of Alaska, North Pacific Fishery Management Council, P.O. Box
1084 103136, Anchorage, AK 99510.
1085 Doyle, M.J. and Mier, K.L. Early life history pelagic exposure profiles of selected
1086 commercially important fish species in the Gulf of Alaska. DSR II
1087 Dumont, H. J., I. Vande Velde, S. Dumont. 1975. The dry weight estimate of biomass in
1088 a selection of cladocera, copepoda and rotifera from the plankton, periphyton and
1089 benthos of continental waters. Oecologia 19: 75-97.
1090 Eggers, D. M. 1977. Nature of Prey Selection by Planktivorous Fish. Ecology 58: 46-59.
1091 Elliott, J. M., W. Davison. 1975. Energy equivalents of oxygen consumption in animal
1092 energetics. Oecologia 19: 195-201.
1093 Elliott, J. M., L. Persson. 1978. The estimation of daily rates of food consumption for
1094 fish. J. Anim. Ecol. 47: 977-991.

1095 Emery, X., 2008. Statistical tests for validating geostatistical simulation algorithms.
1096 Computers & Geosciences 34: 1610–1620.
1097 Ernst, B., Orensanz, J.M., Armstrong, D.A. 2005. Spatial dynamics of female snow crab
1098 (*Chionoecetes opilio*) in the eastern Bering Sea. Can. J. Fish. Aquat. Sci. 62: 250–
1099 268. doi:10.1139/f04-201.
1100 Evans, G.T. 1989. The encounter speed of moving predator and prey. J. Plankton Res.
1101 11: 415-417.
1102 Fox C.J., McCloghrie P., Young E.F., Nash R.D.M. 2006. The importance of individual
1103 behaviour for successful settlement of juvenile plaice (*Pleuronectes platessa* L.):
1104 a modelling and field study in the eastern Irish Sea. Fish Oceanogr 15: 301–313.
1105 Francis, R. I. C. C., Shotton, R. 1997. "Risk" in fisheries management: a review. Can. J.
1106 Fish. Aquat. Sci. 54: 1699– 1715.
1107 Frank, K.T., Carscadden, J.E., Leggett, W.C. 1993. Causes of spatial-temporal variations
1108 in the patchiness of larval fish distributions: differential mortality or behavior.
1109 Fish. Oceanogr. 2: 114-123.
1110 Galindo, H.M., Pfeiffer-Herbert, A.S., McManus, M.A., Chao, Y., Chai, F and Palumbi,
1111 S.R. 2010. Seascape genetics along a steep cline: using genetic patterns to test
1112 predictions of marine larval dispersal. Molecular Ecol., 19: 3692–3707,
1113 Gerritsen, J. and Strickler, J. R. 1977. Encounter probabilities and community structure in
1114 zooplankton: a mathematical model. J. Fish. Res. Bd. Can. 34: 73-82.
1115 Getis, A. and Ord, J.K. 1992, The Analysis of Spatial Association by Use of Distance
1116 Statistics, Geographical Anal. 24: 189-206.
1117 Gustafson, E.J. 1998. Quantifying landscape spatial pattern: what is the state of the art?
1118 Ecosystems 1: 143-156.
1119 Haidvogel D.B., Wilkin J.L., Young R.E., 1991. A semi-spectral primitive equation
1120 ocean circulation model using vertical sigma and orthogonal curvilinear
1121 horizontal coordinates. J. Comput. Phys. 94: 151-185.
1122 Haidvogel, D. B., Arango, H., Hedstrom, K., Beckmann, A., Malanotte-Rizzoli, P.,
1123 Shchepetkin, A., 2000. Model evaluation experiments in the North Atlantic Basin:
1124 Simulations in non-linear terrain-following coordinates. Dyn Atmospheres and
1125 Ocean, 32: 239-281.

1126 Hansson, S., Rudstam, L.G., Kitchell, J.F., Hildén, M., Johnson, B.L.,Peppard, P.E. 1996.
1127 Predation rates by North Sea cod (*Gadus morhua*)—predictions from models on
1128 gastric evacuation and bioenergetics. ICES J. Mar. Sci. 53:107–114.
1129 Hedgecock, D., Barber, P.H., Edmands, S. 2007. Genetic Approaches to Measuring
1130 Connectivity. Oceanography 20: 70-79.
1131 Hermann A.J. and Stabeno P.J. 1996. An eddy-resolving model of circulation on the
1132 western Gulf of Alaska shelf. 1. Model development and sensitivity analyses. J.
1133 Geophys. Res. 101: 1129-1149.
1134 Hermann, A.J., Hinckley, S., Megrey, J.M., Napp, J.M. 2001. Applied and theoretical
1135 considerations for constructing spatially explicit individual-based models of
1136 marine larval fish that include multiple trophic levels. ICES J. Mar. Sci. 58:
1137 1030-1041. doi:10.1006/jmsc.2001
1138 Hewitt, R. 1981. The value of pattern in the distribution of young fish. Rapp. P.-v Reun.
1139 Cons. int. explor. Mer. 178: 229-236.
1140 Hewett, S.W. and Johnson, B.L. 1992. Fish Bioenergetics Model 2, an upgrade of 'A
1141 generalized bioenergetics model of fish growth for microcomputers. University of
1142 Wisconsin Sea Grant Technical Report Number WIS-SG-92-250, 79 pp.
1143 Heywood, D. I., Cornelius, S., and Carver, S. 1998. An introduction to geographical
1144 information systems. New York: Addison Wesley Longman.
1145 Hinckley, S., Bailey, K.H., Picquelle, S.J., Shumacher, J.D., Stabeno, P.J. 1991.
1146 Transport, distribution, and abundance of larval and juvenile walleye pollock
1147 (*Theragra chalcogramma*) in the western Gulf of Alaska. Can. J. Fish. Aquat. Sci.
1148 48: 91-98.
1149 Hinckley S., Hermann A.J., Megrey B.A. 1996. Development of a spatially explicit,
1150 individual-based model of marine fish early life history. Mar. Ecol. Prog. Ser.
1151 139: 47-68.
1152 Hinckley, S., Hermann, A.J., Mier, K.L., Megrey, B.A., 2001. Importance of spawning
1153 location and timing to successful transport to nursery areas: a simulation study of
1154 Gulf of Alaska walleye pollock. ICES J. Mar. Sci. 58: 1042-1052.

1155 Hinrichsen H.H., Möllmann C., Voss R., Köster F.W., Kornilovs. 2002. Biophysical
1156 modeling of larval Baltic cod (*Gadus morhua*) growth and survival. Can. J. Fish.
1157 Aquat. Sci. 59:1858–1873
1158 Hinrichsen, H-H., Schmidt, J. O., Petereit, C., and Mölmann, C. 2005. Survival
1159 probability of Baltic larval cod in relation to spatial overlap patterns with its prey
1160 obtained from drift model studies. ICES J. of Mar. Sci., 62: 878-885.
1161 Holsman, K.K., and Aydin, K. 2015. Comparative methods for evaluating climate
1162 change impacts on the foraging ecology of Alaskan groundfish. Mar. Ecol. Prog.
1163 Ser. 521: 217–235
1164
1165 Horn, H. S. 1966. Measurement of 'overlap' in comparative ecological studies. Am. Nat.,
1166 100: 419-424.
1167
1168 Houde, E.D., and Lovdal, J.D.A. 1985. Patterns of variability in ichthyoplankton
1169 occurrence and abundance in Biscayne Bay, Florida. Est. Coast. Shelf Sci. 20: 79-
1170 103.
1171 Houde, E.D., 1989. Comparative growth, mortality, and energetic of marine fish larvae:
1172 temperature and implied latitudinal effects. Fish. Bull. US 87: 471-495.
1173 Huebert, KB. and Sponaugle, S. 2009. Observed and simulated swimming trajectories of
1174 late-stage coral reef fish larvae off the Florida Keys. Aquat. Biol. 7: 207–216.
1175 doi: 10.3354/ab00200
1176 Hurst, T. 2007. Thermal effects on behavior of juvenile walleye Pollock (Theragra
1177 chalcogramma): implications for energetics and food web models. Can. J. Fish.
1178 Aquat.Sci. 64: 449-457.
1179 Kareiva, P.M. and Shigesada, N., 1983. Analyzing insect movement as a correlated
1180 random walk. Oecologia. 56: 234-238.
1181 Kell, L. T., Pastoors, M. A., Scott, R. D., Smith, M. T., Van Beek, F. A., O'Brien, C. M.,
1182 and Pilling, G. M. 2005a. Evaluation of multiple management objectives for
1183 Northeast Atlantic flatfish stocks: sustainability vs. stability of yield. ICES J. Mar.
1184 Sci. 62: 1104–1117.
1185 Kell, L. T., Pilling, G. M., Kirkwood, G. P., Pastoors, M., Mesnil, B., Korsbrekke, K.,
1186 Abaunza, P. 2005b. An evaluation of the implicit management procedure used for
1187 some ICES groundfish stocks. ICES J. of Mar. Sci., 62: 750–759.

1188 Kell, L.T., Mosqueira, I., Grosjean, P., Fromentin, J-M., Garcia, D., Hillary, R., Jardim,
1189 E., Mardle, S., Pastoors, M.A., Poos, J. J., Scott, F., and Scott, R.D. 2007. FLR:
1190 an open-source framework for the evaluation and development of management
1191 strategies. – ICES J. of Mar. Sci., 64: 640 –646.
1192 Kendall, A.W., CIarke, M.E., Yoklavich, M.M., Boehlert, G.W. 1987. Distribution,
1193 feeding, and growth of larval walleye pollock, *Theragra chalcogramma*, from
1194 Shelikof Strait, Gulf of Alaska. Fish. Bull. US 85: 499-521.
1195 Kendall, A.W., Incze, L.S., Ortner, P.B., Cummings, S.R., Brown, P.K., 1994. The
1196 vertical distribution of eggs and larvae of walleye pollock (*Theragra*
1197 *chalcogramma*) in Shelikof Strait, Gulf of Alaska. Fish. Bull. US 92: 540-554.
1198 Kendall, A.W., Jr., Perry, R.I., and Kim, S. 1996 (eds) 1996. Fisheries oceanography of
1199 walleye pollock in Shelikof Strait, Alaska. Fish. Oceanogr. 5 (Suppl. 1), 203p.
1200 Kosfeld, R. and Lauridsen, J. 2012. Identifying clusters within R&D intensive industries
1201 using local spatial methods, Joint Discussion Paper Series in Economics, No. 14-
1202 2012.
1203 Kwan, M. 2012. "The uncertain geographic context problem". Annals of the Association
1204 of American Geographers 102: 958–968. doi:10.1080/00045608.2012.687349.
1205 Lang, G.M., Brodeur, R.D., Napp, J.M. 2000. Variation in groundfish predation on
1206 juvenile walleye pollock relative to hydrographic structure near the Pribilof
1207 Islands, Alaska. ICES J. Mar. Sci. 57: 265-271.
1208 Lantuéjoul, C. 2002. Geostatistical Simulation: Models and Algorithms. Springer, Berlin.
1209 256 pp.
1210 Lett, C., Verley, P., Mullon, C., Parada, C., Brochier, T., Penven, P., Blake, B. 2008. A
1211 Lagrangian tool for modelling ichthyoplankton dynamics. Environmental
1212 Modelling & Software, 23: 1210-1214.
1213 Link J. and Edsall, T.A. 1996. The effect of light on lake herring (*Coregonus artedi*)
1214 reactive volume. Hydrobiologia 332: 131-140.
1215 Lloyd M. 1967. Mean crowding. I. Anim. Ecol. 36:1-30.
1216 Lynch, D.R. 2009. Skill assessment for coupled biological/physical models of marine
1217 systems. J. of Mar. Syst. 76: 1-3.

1218 MacKenzie, B.R., Leggett, W.C., Peters, R.H. 1990. Estimating larval fish ingestion
1219 rates: can laboratory derived values be reliably extrapolated to the wild? Mar.
1220 Ecol. Prog. Ser. 67: 209-225.
1221 Matarese, A.C., Blood, D.M., Picquelle, S.J., Benson, J.L.. 2003. Atlas of abundance and
1222 distribution patterns of ichthyoplankton from the northeast Pacific Ocean and
1223 Bering Sea ecosystems based on research conducted by the Alaska Fisheries
1224 Science Center (1972-1996). NOAA Prof. Paper NMFS 1, 281 p.
1225 Matsuura, Y., and Hewitt, R. 1995. Changes in the spatial patchiness of Pacific
1226 mackerel, *Scomber japonicus*, larvae with increasing age and size. Fish. Bull. 93:
1227 172-178.
1228 Mazur, M. M., and Beauchamp, D.A. 2006. Linking piscivory to spatial-temporal
1229 distributions of pelagic prey fishes with a visual foraging model. J. Fish Biol. 69:
1230 151-175.
1231 Mazur, M.M., Wilson, M.T., Dougherty, A.B., Buchheister, A, Beauchamp, D.A., 2007.
1232 Temperature and prey quality effects on growth of juvenile walleye pollock
1233 *Theragra chalcogramma*: a spatially explicit bioenergetics approach. J. Fish.
1234 Biol.70: 816-136.
1235 Megrey, B.A. and Hinckley, S. 2001. Effect of turbulence of larval fishes: a sensitivity
1236 analysis using an individual-based model. ICES J. Mar. Sci. 58: 1015-1029.
1237 Merati, N. And Brodeur, R. D. 1996. Feeding habits and daily ration of juvenile walleye
1238 pollock, *Theragra chalcogramma*, in the western Gulf of Alaska. In Ecology of
1239 juvenile walleye pollock*, Theragra chalcogramma* (Brodeur, R. D., Livingston, P.
1240 A., Loughlin, T. R., Hollowed, A. B. eds), pp.65-79. U.S. Department of
1241 Commerce, NOAA Technical Report NMFS 126.
1242 Methot, R.D. 1986. Frame trawl for sampling pelagic juvenile fish. Cal. Coop. Oceanic
1243 Fish. Invest. (CalCOFI) Rep. 27: 267-278.
1244 North, E.W., Gallego, A., Petitgas, P.. 2009. Manual of recommended practices for
1245 modeling physical-biological interactions during fish early life. ICES Coop. Res.
1246 Rep. No. 295.
1247 Ord, A. and Getis, J.K. 1995. Local spatial autocorrelation statistics: distributional issues
1248 and an application. Geographical Anal. 27: 286-306.

1249 Palumbi S.R. 2003. Population genetics, demographic connectivity, and the design of
1250 marine reserves. Ecol. Applications 13: 146-158.
1251 Parada, C., Horne, J.K., Hinckley, S., Curchitser, E, Hermann, A.J., Mazur, M. (This
1252 issue) Modeling connectivity of walleye pollock in the Gulf of Alaska: Linkages
1253 to Bering Sea and stock structure implications. Deep Sea Res. II GOAIERP
1254 Special Issue.
1255 Pedersen, O.P., Nilssen, E.M., Jørgensen, L.L., Slagstad, D. 2006. Advection of the Red
1256 King Crab larvae on the coast of North Norway—A Lagrangian model study.
1257 Fisheries Research 79: 325–336
1258 Peterman, R. M. 2004. Possible solutions to some challenges facing fisheries scientists
1259 and managers. ICES J. Mar. Sci. 61: 1331– 1343.
1260 Petrik, C.M., Duffy-Anderson, J.T., Mueter, F., Hedstrom, K., Curchitser, E.N. 2014.
1261 Biophysical transport model suggests climate variability determines distribution
1262 of Walleye Pollock early life stages in the eastern Bering Sea through effects on
1263 spawning. Prog. Oceanogr., http://dx.doi.org/10.1016/j.pocean.2014.06.004
1264 Punt, A. E. 2006. The FAO Precautionary Approach after almost 10 years: have we
1265 progressed towards implementing simulation-tested feedback-control
1266 management systems for fisheries management? Nat. Resource Modeling, 19:
1267 441– 464.
1268 Radach, G., and Moll, A. 2006. Review of three-dimensional ecological modelling
1269 related to the North Sea shelf system - Part 2: Model validation and data needs.
1270 Oceanography and Marine Biology; an Annual Review, 44: 1–60.
1271 Rose, K.A., Roth, B.M., Smith, E.P. 2009. Skill assessment of spatial maps for
1272 oceanographic modeling. J. Mar. Syst. 76: 34-48.
1273 Rosenberg, A. A., and Restrepo, V. R. 1994. Uncertainty and risk evaluation in stock
1274 assessment advice for US marine fisheries. Can. J. Fish. Aquat. Sci. 51: 2715–
1275 2720.
1276 Schabetsberger, R., Sztatecsny, M., Drozdowski, G., Brodeur, R.D., Swartzman, G.L.,
1277 Wilson, M.T., Winter, A., G., Napp, J.M. 2003. Size-dependent, spatial, and
1278 temporal variability of juvenile walleye pollock (*Theragra chalcogramma*)
1279 feeding at a structural front in the southeast Bering Sea. Mar. Ecol. 24: 141–164.

1280 Scheffer, M., Baveco, J. M., DeAngelis, D. L., Rose, K. A., Van Nes, E. H. 1995. Super-
1281 individuals: a simple solution for modelling large populations on an individual
1282 basis. Ecol. Mod. 80: 161–170.
1283 Schumacher, J.D. and Kendall, A.W. Jr., 1991. Some interactions between young pollock
1284 and their environment in the western Gulf of Alaska. Calif. Coop. Oceanic. Fish.
1285 Invest. Rep. 32: 22-40.
1286 Selkoe, K.A., Henzler, C.M., Gaines, S.D. 2008. Seascape genetics and the spatial
1287 ecology of marine populations. Fish and Fisheries 9: 363-377.
1288 Shchepetkin, A.F., McWilliams, J.C. 2005. The Regional Ocean Modelling System: a
1289 split-explicit, free-surface, topography following coordinates ocean model. Ocean
1290 Modelling, 9: 347–404.
1291 Siddon, E.C., Kristiansen, T., Mueter, F.J., Holsman, K.K., Heintz, R.A., Farley, E.V.
1292 2013. Spatial Match-Mismatch between Juvenile Fish and Prey Provides a
1293 Mechanism for Recruitment Variability across Contrasting Climate Conditions in
1294 the Eastern Bering Sea. PLOS One. 8(12): 1-13.
1295 Siniff, D. P. and Jessen, C. R. 1969. A simulation model of animal movement patterns.
1296 Adv. Ecol. Res. 6: 185 –219.
1297 Skellam, J. G. 1973. The formulation and interpretation of mathematical models of
1298 diffusionary processes in population biology. In: The mathematical theory of the
1299 dynamics of biological populations (eds. M. S. Bartlett and R. W. Hiorns), pp.
1300 63–85. London, UK: Academic Press.
1301 Søiland, H., and Skogen, M. D. 2000. Validation of a three-dimensional biophysical
1302 model using nutrient observations in the North Sea. – ICES J. Mar. Sci. 57: 816–
1303 823.
1304 Spring. S. and Bailey, K.M. 1991. Distribution and abundance of juvenile pollock from
1305 historical shrimp trawl surveys in the western Gulf of Alaska. AFSC Processed
1306 Report 91-18, 66p. Alaska Fish. Sci. Cent., Natl. Mar. Fish. Serv., NOAA, 7600
1307 Sand Point Way NE, Seattle WA 98115.
1308 Sogard, S. M. and Olla, B. L. 2000. Endurance of simulated winter conditions by age-0
1309 walleye pollock: effects of body size, water temperature and energy stores. J.
1310 Fish. Biol. 56: 1-21.

1311 Stabeno P.J. and Hermann A.J. 1996. An eddy resolving model of circulation on the
1312 western Gulf of Alaska shelf. II. Comparison of results to oceanic observations. J.
1313 Geophys. Res. 101: 1151-1161.
1314 Staaterman, E., and C.B. Paris. 2014. Modelling larval fish navigation: the way forward.
1315 ICES J. of Mar. Sci. 71(4): 918–924.
1316 Stockhausen, W. T. and Hermann, A.J. 2007. Modeling larval dispersion of rockfish: a
1317 tool for marine reserve design? Pp. 251-273 in Biology, Assessment, and
1318 Management of North Pacific Rockfishes. Alaska Sea Grant College Program,
1319 AK-SG-07-01.
1320 Stockwell, J.D. and Johnson, B.M. 1997. Refinement and calibration of a bioenergetics-
1321 based foraging model for kokanee. Can. J. Fish. Aquat. Sci. 54: 2659-2676.
1322 Stockwell, J.D., and Johnson, B.M. 1999. Field evaluation of a bioenergetics-based
1323 foraging model for kokanee (*Oncorhynchus nerka*). Can. J. Fish. Aquat. Sci.
1324 56(Suppl. 1): 140-151.
1325 Stow, C.A., Jolliff, J., McGillicuddy, D.J.Jr., Doney, S.C., Allen, J.I., Friedrichs,
1326 M.A.M., Rose, K.A., Wallhead, P. 2009. Skill assessment for coupled
1327 biological/physical models of marine systems. J. Mar. Sys. 76: 4-15.
1328 Sundby. S., 1983. A one-dimensional model for the vertical distribution of pelagic fish
1329 eggs in the mixed layer. Deep Sea Res. 30: 645-661.
1330 Svetlichny, L.S. and Hubareva, E.S. 2005. The energetics of *Calanus euxinus*:
1331 locomotion, filtration of food and specific dynamic action. J. of Plankton Res. 27:
1332 671-682.
1333 Syrjala, S. E. 1996. A statistical test for a difference between the spatial distributions of
1334 two populations. Ecology 77: 75-80.
1335 Taylor, K.E. 2001. Summarizing multiple aspects of model performance in a single
1336 diagram. J. Geophysical Res., 106: 7183–7192.
1337 Thorrold, S.R., Latkoczy, C., Swart, P.K., Jones, C.M. 2001. Natal homing in a marine
1338 fish metapopulation. Science 291: 297-299
1339 Turchin, P. 1998. Quantitative analysis of movement: measuring and modeling
1340 population redistribution in animals and plants. Sunderland, MA: Sinauer
1341 Associates.

1342 Utne, K.R. and Huse, Geir. 2012. Estimating the horizontal and temporal overlap of
1343 pelagic fish distribution in the Norwegian Sea using individual-based modelling,
1344 Marine Biology Research, 8:5-6, 548-567, DOI: 10.1080/17451000.2011.639781
1345 Vikebø, F., Sundby, S., Adlandsvik, B, Fiksen, Ø. 2005. The combined effect of
1346 transport and temperature on distribution and growth of larvae and pelagic
1347 juveniles of Arcto-Norwegian cod. ICES J. Mar. Sci. 62: 1375-1386.
1348 doi:10.1016/j.icesjms.2005.05.017
1349 Vikebø, F., Jørgensen, C., Kristiansen, T, Fiksen, Ø. 2007. Drift, growth, and survival of
1350 larval Northeast Arctic cod with simple rules of behavior. 347: 207–219, doi:
1351 10.3354/meps06979
1352 Warner, J. C., Geyer, W. R., Lerczak, J. A. 2005. Numerical modeling of an estuary: A
1353 comprehensive skill assessment. J. Geophys. Res. v.110, C05001,
1354 doi:10.1029/2004JC002691
1355 Werner F.E., Perry R.I., Lough R.G., Naimie C.E. 1996. Trophodynamic and advective
1356 influences on Georges Bank larval cod and haddock. Deep-Sea Res II 43:1793–
1357 1822.
1358 Werner F.E., Quinlan J.A., Lough R.G., Lynch D.R. 2001. Spatially-explicit individual
1359 based modeling of marine populations: a review of the advances in the 1990s.
1360 Sarsia 86: 411–421.
1361 Wiedmann, M.A., Pedersen, O.-P., Nilssen, E.M. 2012. The recruitment process of the
1362 Barents Sea capelin (*Mallotus villosus*) stock, 2001–2003. Fish. Oceanogr. 21(6):
1363 379–392.
1364 Willis, J. 2011.Modelling swimming aquatic animals in hydrodynamic models.
1365 Ecological Modelling, 222: 3869–3887.)
1366 Wilson, M.T., Brodeur, R.D., Hinckley, S. 1996. Distribution and abundance of age-0
1367 walleye pollock, Theragra chalcogramma, in the western Gulf of Alaska during
1368 September 1990. In: Brodeur, R.D., Livingston, P.A., Loughlin, T.R., Hollowed,
1369 A.B. (eds) Ecology of Juvenile Walleye pollock , Theragra chalcogramma, U.S.
1370 Dep. Comm., NOAA Tech. Rep. NMFS 126 p 11-24.

1371 Wilson, M.T. 2000. Effects of year and region on the abundance and size of age-0
1372 walleye pollock, *Theragra chalcogramma*, in the western Gulf of Alaska, 1985-
1373 1988. Fish. Bull. U.S. 98: 823-834.
1374 Wilson, M.T., Jump, C.M., Duffy-Anderson, J.T., 2006. Comparative analysis of the
1375 feeding ecology of two pelagic forage fishes: capelin *Mallotus villosus* and
1376 walleye pollock *Theragra chalcogramma*. Mar. Ecol. Prog. Series 317: 245-258.
1377 Winter, A., Swartzman, G., Ciannelli, L. 2005. Early- to late- summer population growth
1378 and prey consumption by age-0 pollock, in two years of contrasting pollock
1379 abundance near the Pribilof Islands, Bering Sea. Fish. Oceanogr. 14: 307-320.
1380 Woillez, M. 2007. Contributions géostatistiques à la biologie halieutique. Thèse de
1381 Docteur en Géostatistique, Ecole Nationale Supérieure des Mines de Paris,
1382 France. 175 pp.
1383 Woillez, M., Poulard, J-C., Rivoirard, J., Petitgas, P., Bez, N. 2007. Indices for capturing
1384 spatial patterns and their evolution in time, with application to European hake
1385 (*Merluccius merluccius*) in the Bay of Biscay. – ICES J. Mar. Sci. 64: 537-550.
1386 Woillez, M., Rivoirard, J., Petitgas, P. 2009. Notes on survey-based spatial indicators for
1387 monitoring fish populations. Aquat. Living Resources, 22: 155-164.
1388 Woillez, M., Rivoirard, J., Fernandes, P. 2009. Evaluating the uncertainty of abundance
1389 estimates from acoustic surveys using geostatistical simulations. – ICES J. Mar.
1390 Sci. 66: 1377-1383.
1391 Yamashita, Y., Bailey, K.M., 1989. A laboratory study of the bioenergetics of larval
1392 walleye pollock, *Theragra chalcogramma*. Fish. Bull. US 87: 525-536.
1393 Zacherl, D.C., Manriquez, P.H., Paradis, G., Day, R.W., Castilla, J.C, Warner R.R., Lea
1394 D.W., Gaines, S.D. 2003. Trace elemental fingerprinting of gastropod statoliths
1395 to study larval dispersal trajectories. Mar. Ecol. Prog. Ser. 248: 297-303

Table 1. Parameters and feeding model for juvenile walleye pollock.

| Parameters and units | Symbol | Functions/Values | References. |
|---|---|---|---|
| Prey types | $k$ | $k$=1, euphausids<br>$k$=2, large copepods<br>$k$=3, small copepods | |
| Density of prey $k$ (num $m^{-3}$) | $N_k$ | | Hinckley, 1999 |
| Offshelf area | | Prey set to 0 | |
| Inner shelf areas | | 1.17838 ($k$=1)<br>66.6632 ($k$=2)<br>486.277 ($k$=3) | |
| Mid and outer shelf jd** <120) | | 0.29459 ($k$=1)<br>16.6659 ($k$=2)<br>121.569 ($k$=3) | |
| 120<=jd**<160 | | Linear increase to inner shelf values | |
| Pollock size class (mm) | $j$ | $j$=1:3 | |
| Probability of preference for prey $k$ size j | $P_{kj}$ | 0.0000 ($k$=1, $j$=1*)<br>0.1429 ($k$=1, $j$=2*)<br>0.8571 ($k$=1, $j$=3*)<br>0.1270 ($k$=2, $j$=1*)<br>0.2381 ($k$=2, $j$=2*)<br>0.6349 ($k$=2, $j$=3*)<br>0.6481 ($k$=3, $j$=1*)<br>0.3242 ($k$=3, $j$=2*)<br>0.0278 ($k$=3, $j$=3*) | Wilson et al. (2006) |
| Pollock mean swim speed ($ms^{-1}$) | $\bar{x}$ | 0.15 | Sogard and Olla (2000) |
| Prey k swim speed ($ms^{-1}$) | $v_k$ | 0.0285 ($k$=1)<br>0.0100 ($k$=2)<br>0.0020 ($k$=3) | De Robertis et al. (2003) |
| Conversion factor to hours | $A$ | 1/60 | |
| Handling time (seconds $prey^{-1}$) | $t_h$ | 0.33 | Stockwell and Johnson (1997) |
| Reactive distance (m) | $d_c$ | 0.1 | Link and Edsall (1996) |

| | | | |
|---|---|---|---|
| Mean weight of prey *k* (g) | $\bar{W}_k$ | 0.0402 (*k*=1)<br>$5.674 \times 10^{-4}$ (*k*=2)<br>$1.122 \times 10^{-4}$ (*k*=3) | Winter el al. (2005),<br>Dumont et al. (1975)<br>Dumont et al. (1975) |
| Stomach capacity Initialization | $St_h$ | 0.2Cmax*** | Mazur, M. Pers. Comm. |
| Number of prey *k* eaten in *h* hours | $E_{k,h}$ | $E_{k,h=} \sum_j \left( \frac{S_k N_k P_{jk}}{1 + S_k t_h a} \right)$ | Gerritsen and Strickler (1977),, Stockwell and Johnson (1997) |
| Search volume of pollock searching for prey *k* | $S_k$ | $S_{k=} \pi d^2 \sqrt{\bar{x}^2 + v_k^2}$ | Evans (1989) |
| Total biomass eaten by hour | $G_h$ | $G_h = \sum_k E_{k,h} \bar{W}_k$ | Eggers (1977) |
| Digestion per hour | $D_h$ | $D_h = St_{h+} G_h - St_h e^{d_c} + \frac{G_h}{d_c}(1 - e^{d_c})$ | Elliott and Persson (1978),<br>Bevelhimer and Adams (1993) |

*Corresponds to juvenile pollock size classes where *j=1*: 25mm <= length < 40, j=2: 120mm > length >= 40mm and j=3: length >= 120mm.
**jd=Julian days
***Cmax= maximum consumption based on Hinckley et al., (2002)
W=weight (g), T=temperature (°C)

Table 2. Parameters in the bioenergetics model for juvenile walleye pollock.

| **Parameter description and units** | **Symbol** | **Values** | **Reference** |
|---|---|---|---|
| **Consumption ($gg^{-1}$ $day^{-1}$)** | *C* | | |
| Proportion of maximum consumption | *P* | 0-2 | 1 |
| Intercept of the allometric function | *Ac* | 0.38 | 1 |
| Slope of the allometric function | *Bc* | 0.68 | 1 |
| Temperature dependence coefficient | *Qc* | 2.6 | 1 |
| Optimum temperature for consumption ($^oC$) | *Tco* | 10 | 1 |
| Maximum temperature for consumption ($^oC$) | *Tcm* | 15 | 1 |
| | | | |
| **Respiration ($gg^{-1}$ $0_2$ $day^{-1}$)** | *R* | | |
| Intercept of the allometric function | *Ar* | 0.0075 | 1 |
| Slope of the allometric function | *Br* | 0.251 | 1 |
| Temperature dependence coefficient | *Qr* | 2.6 | 1 |
| Optimum temperature for respiration($^oC$) | *Tro* | 13 | 1 |
| Maximum temperature for respiration ($^oC$) | *Trm* | 18 | 1 |
| Proportion of assimilated energy lost for Specific Dynamic Action | *Ds* | 0.125 | 1 |
| Multiplier for active metabolism | *Am* | 1 | 1 |
| Respiration in Joules | *Rj* | | |
| Conversion from g of oxygen to joules | *convj* | 13560 | 2 |
| | | | |
| **Egestion** | *F* | | |
| Proportion consumed energy | *Fa* | 0.15 | 1 |
| | | | |
| **Excretion** | *U* | | |
| Proportion of assimilated energy | *Ua* | 0.11 | 1 |

(1) Ciannelli et al. (1998), (2) Elliott and Davison (1975)

Table 3. Daily mortality rates for egg, larvae and juveniles of walleye pollock used for IBM experiments.

| Year | Eggs* | Feeding larvae* | Juveniles** |
|---|---|---|---|
| 1987 | 0.226 | 0.064 | 0.00005 |
| 1988 | 0.300 | 0.036 | - |
| 1989 | 0.170 | 0.157 | - |
| 1990 | 0.150 | 0.073 | 0.01400 |
| 1991 | 0.220 | 0.126 | - |
| 1992 | 0.184 | 0.049 | - |
| 1993 | - | 0.038 | 0.00607 |
| 1994 | - | 0.057 | - |
| 1996 | - | 0.037 | 0.01076 |
| 1999 | - | - | 0.00157 |
| 2001 | - | - | 0.00353 |
| Other | 0.205*** | 0.0200*** | 0.00509 |

*For egg and larval daily mortality rates for pollock and methods of calculations, see Bailey et al. 1996.
** Juvenile daily mortality was inferred from stomach contents from groundfish consumption and normalized to a maximum mortality, for missing values we used an average of the available data.
*** Average values for missing years (Bailey, pers. comm.)

Table 4. Results of the Syrjala tests on the three sets of model vs. survey information, based on 1000 permutations. Test uses normalized densities.

| | May survey vs. model | June/July survey vs. model | August/September survey vs. model |
|---|---|---|---|
| | | Cramer-von Mises test | |
| Test statistic | 0.591 | 1.232 | 1.399 |
| P-value | 0.417 | 0.023* | 0.064 |
| N | 13 | 94 | 49 |
| | | Kolmogorov-Smirnov test | |
| Test statistic | 0.405 | 0.319 | 0.452 |
| P-value | 0.353 | 0.019* | 0.058 |
| N | 13 | 94 | 49 |

* Significant at p=0.05 (Spatial distributions are different)

Table 5. Comparison of indices characterizing spatial distributions of pollock from the survey data and the IBM for June/July and August/September. Lower (lci: 2.5%) and upper (uci: 97.5%) confidence intervals associated with spatial indices computed from the survey data are shown. Values of spatial indices included within the confidence intervals appear shaded in grey. Longitude (in km, xcg) and latitude (in km, ycg) of the center of gravity, inertia (I), isotropy (Iso), positive area (pa), spreading area (sa) and equivalent area (ea) are the spatial indices used to describe each spatial distribution. Release spawning months (April, May) and areas (Area 8, North Shelikof Strait; Area 11, Shelikof Exit area) were tested.

| | **Spatial Indices** | | **xcg** | **ycg** | **I** | **Iso** | **pa** | **sa** | **ea** |
|---|---|---|---|---|---|---|---|---|---|
| | | | (June/July spatial distribution) | | | | | | |
| Survey | lci | | -383 | 6183 | 45146 | 0,149 | 75000 | 33744 | 34331 |
| | uci | | -289 | 6221 | 81629 | 0,218 | 90178 | 42528 | 43293 |
| | data | | -352 | 6199 | 53347 | 0,165 | 84789 | 38756 | 38437 |
| Model | April | area 8 | -338 | 6228 | 5319 | 0,186 | 1900 | 833 | 731 |
| | | area 11 | -343 | 6212 | 7412 | 0,276 | 1900 | 1049 | 981 |
| | | areas 8 & 11 | -342 | 6215 | 7136 | 0,273 | 3200 | 1183 | 1040 |
| | May | area 8 | -361 | 6193 | 8668 | 0,370 | 1800 | 1233 | 1313 |
| | | area 11 | -444 | 6181 | 19914 | 0,245 | 2900 | 1849 | 1840 |
| | | areas 8 & 11 | -423 | 6184 | 18452 | 0,255 | 4100 | 2393 | 2336 |
| | April & May | area 8 | -356 | 6201 | 8216 | 0,371 | 3200 | 1498 | 1557 |
| | | area 11 | -408 | 6192 | 18042 | 0,252 | 4100 | 2238 | 2144 |
| | | areas 8 & 11 | -397 | 6194 | 16413 | 0,264 | 6000 | 2692 | 2297 |
| | | | (August/September spatial distribution) | | | | | | |
| Survey | lci | | -261 | 6209 | 14504 | 0,297 | 101645 | 30191 | 27815 |
| | uci | | -218 | 6231 | 23930 | 0,426 | 120555 | 38365 | 37140 |
| | data | | -241 | 6221 | 13693 | 0,386 | 111506 | 32988 | 28490 |
| Model | April | area 8 | -342 | 6211 | 4553 | 0,243 | 1600 | 647 | 505 |
| | | area 11 | -300 | 6215 | 6203 | 0,387 | 2500 | 1469 | 1166 |
| | | areas 8 & 11 | -306 | 6214 | 6181 | 0,377 | 3600 | 1508 | 1062 |
| | May | area 8 | -268 | 6212 | 2032 | 0,460 | 2500 | 1840 | 2011 |
| | | area 11 | -301 | 6192 | 15578 | 0,204 | 4900 | 3051 | 3147 |
| | | areas 8 & 11 | -294 | 6196 | 12925 | 0,217 | 6200 | 3867 | 3989 |
| | April & May | area 8 | -282 | 6212 | 3295 | 0,429 | 3900 | 2091 | 2221 |
| | | area 11 | -301 | 6198 | 13263 | 0,250 | 6700 | 3707 | 3050 |
| | | areas 8 & 11 | -297 | 6201 | 11377 | 0,262 | 9000 | 4462 | 3474 |

Table 6. Methods used in this study to compare modeled vs. survey distributions. Listed are attributes that are addressed, and considerations/constraints in using these methods.

| **Method** | **Attribute Addressed** | **Constraints/Considerations** |
|---|---|---|
| Weighted Centroids | Center of gravity of a spatial distribution | Global measure. May be effected by sampling design (surveys) or initial conditions and modeling domain (IBM). Useful for initial visual comparison. May be effected by outliers. |
| Inertia | Variance of a spatial distribution | Global measure. |
| Directional Ellipses | Orientation of 1 standard deviation ellipse around center of gravity | Global measure. May be affected by directionality/heterogeneity of currents. Useful for visual comparison. May be effected by outliers. |
| Isotropy | Evenness of dispersion of a spatial distribution | May be affected by currents (and hydrodynamic model match/mismatch) and topography |
| Positive, Spreading and Equivalent Area | Area occupied by positive densities, proportional area occupied per unit area, area occupied if all cells had the same density | Affected by differences in measured vs. modeled currents. Affected by IBM initial conditions. |
| Getis-Ord Gi* | Spatial clustering of georeferenced data, into clusters of high values (hotspots) and low values (coldspots) | Small scale features may be in different places in model output versus data because of hydrodynamics model mismatch. Results not reliable with too few values (<30). All features should have at least one neighbor. No feature should have all other features as neighbors. Chosen scale important. Spatial clustering may imply underlying spatial processes. |
| NDI | Normalized difference index | Strongly affected by bin size. Indicates where model values are greater than data and vs. |
| OC | Overlap coefficient | Strongly affected by bin size. |
| Syrjala | Nonparametric statistical tests of the null hypothesis that the spatial distribution of two populations is the same. | Global measure. May be affected by bin size. KS test is sensitive to small numbers of extreme values. Does not compare levels of abundance. Easy to implement. |

| Method | Attribute Addressed | Constraints/Considerations |
|---|---|---|
| Geostatistical Comparison of Spatial Indices | Allows tests of whether spatial indices from model/data are significantly different | Appropriate implementation and validation of simulation components important. If currents very heterogeneous, area occupied indices may not match. Initial conditions must be as accurate as possible. |

Table 7. Summary of results of methods used to compare IBM output and survey data.

| Method | Results |
|---|---|
| Centroids | (May) Data: Centroid near of Sutwik I.<br>Model: Centroid near Sutwik I.<br>(June/July) Data: Centroid just east of Shumagins Is.<br>Model: Centroids just east of Shumagin Is.<br>(Aug/Sept) Data: Centroid shoreward of Shumagin Is.<br>Model: Centroids shoreward of Shumagin Is.<br>(Spatial Indices Test)<br>June/July: 12 indices (of 18) within 95% CI<br>Aug/Sept: (5 of 18) within 95% CI |
| Inertia | (May) Survey spread smaller than model due to reduced survey area<br>(June/July) Spread similar<br>(Aug/Sept) Survey spread larger than model spread due to exclusion of Kodiak area fish<br>(Spatial Indices Test)<br>June/July: 0 of 9 within 95% CI<br>Aug/Sept: 1 of 9 within 95% CI |
| Directional Ellipses | All model and surveys oriented along Alaska Peninsula |
| Isotropy | (Spatial Indices Test)<br>June/July: 1 of 9 within 95% CI<br>Aug/Sep: 2 of 9 within 95% CI |
| Positive Area, Spreading Area, Equivalent Area | (Spatial Indices Test)<br>June/July: 0 of 27 within 95% CI<br>Aug/Sept: 0 of 27 within 95% CI |
| Getis-Ord Gi* | (May) Data: Hotspots present<br>Model: Few hotspots present<br>(June/July) Data: Hotspots between Sutwik-Shumagin Is., especially inshore of Shumagins<br>Model: Coldspot inshore of Shumagins, hotspot just west of Shumagins<br>(Aug/Sept) Data: Hotspots near Sutwik, inshore & west of Shumagins<br>Model: Coldspot inshore of Shumagins, hotspots west of Shumagins |
| NDI | (May) Low coverage, some areas of difference<br>(June/July) Low differences except in a few areas near Shumagins<br>(Aug/Sept) Some differences near Shumagins<br>(All time periods) Data values higher than model |
| OC | (May) Locally high areas of overlap<br>(June/July) Higher overlap, esp. between Sutwik and Shumagins<br>(Aug/Sept) Lowest overall overlap, high overlap near Shumagin Is. |

| | | |
|---|---|---|
| Syrjala | (May) for | No signifigant difference between survey and model |
| | | both CvM and KS tests |
| | (June/July) | Significant differences for both tests at p=0.05 |
| | (Aug/Sept) | No significant differences for both tests |

List of Figures

Figure 9. Distribution of Getis-Ord Gi*statistics from the survey and the model output for June/July, 1987.

Figure 10. Distribution of Getis-Ord Gi* statistics from the survey and the model output for August/September, 1987.

Figure 11. Normalized difference indices (NDI) for the three time periods (rows) and bin sizes (column). Small differences are indicated by hotter colors (lower numbers) and larger differences by cooler colors (higher numbers). Overall NDIs are shown in the lower right of each panel.

Figure 12. Overlap coefficient (OC) for three time periods (rows) and bin sizes (columns). Cooler colors (higher numbers) indicate higher overlap, while warmer colors (lower numbers) indicate lower overlap. Overall OCs (labeled C) are shown in the lower right corner of each panel.

Figure 13. (a) Linear interpolation model for the normal score transformation of the pollock densities sampled in June/July. (b) Idem for the August/ September survey. (c) The experimental variogram of the normal score variable for the June/July survey with circles proportional to number of data is shown in light grey. The model of the Gaussian variable and the corresponding expression for the normal score variable are represented, respectively, by a dashed and solid black line. The experimental variogram of the Gaussian variable with circles proportional to number of values, obtained after the Gibbs sampling, is represented in dark grey and is consistent with the Gaussian model. (d) Idem for the August/September survey.

Figure 14. Top: three realizations (max., med., and min.) of spatial average density values, respectively a, b, and c) of the pollock densities in June/July. Bottom: three realizations (max., med. and min.) of spatial average density values, respectively d, e, and f) of young pollock densities in August/September. Only simulated values above zero have been colored. As examples of the computation of spatial indices from those simulated fields, the center of gravity and axes of inertia have been represented in white.

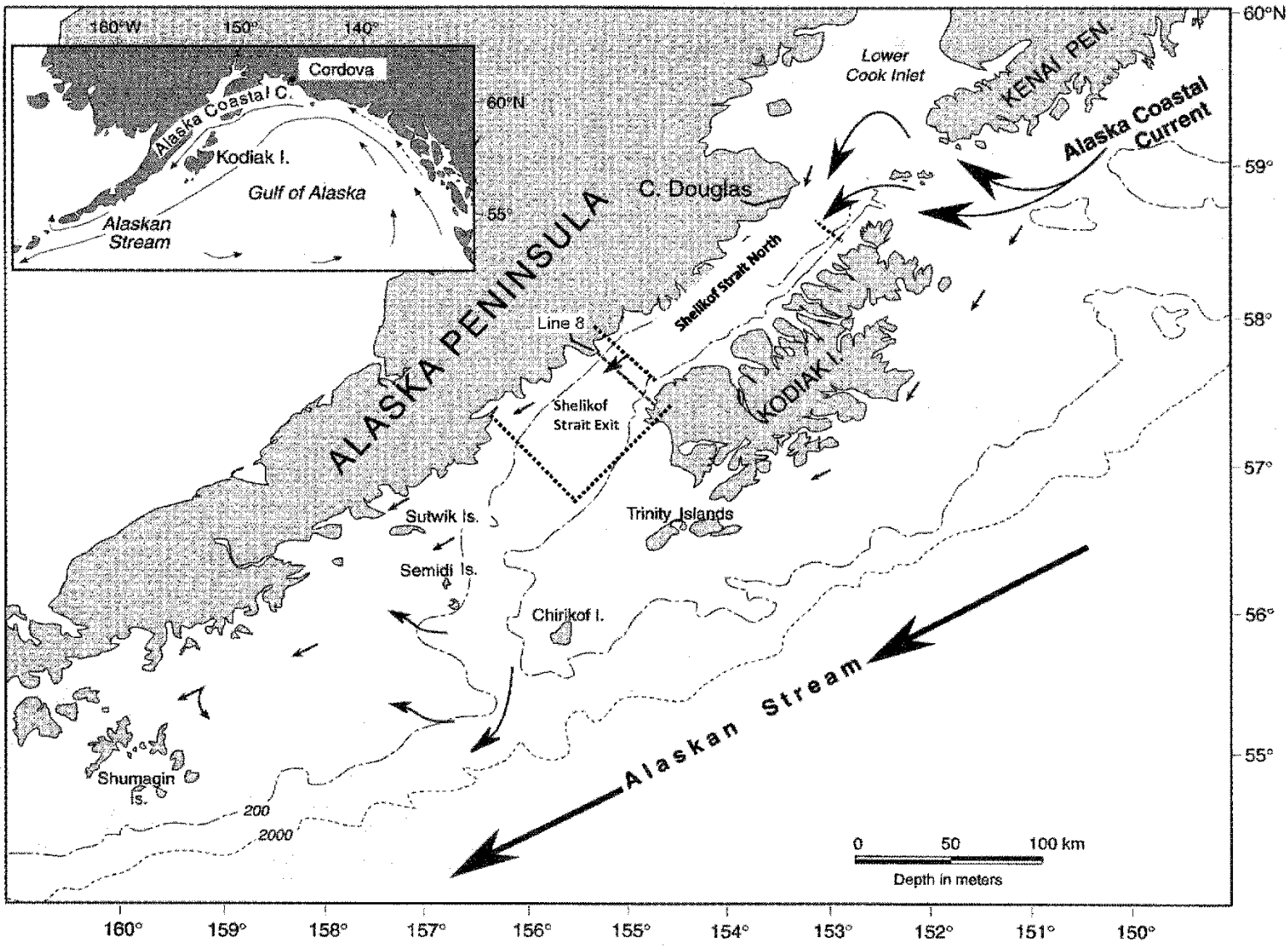
160°W
150°
140°
60°N
55°
Cordova
Alaska Coastal C.
Kodiak I.
Gulf of Alaska
Alaskan Stream
Lower Cook Inlet
KENAI PEN.
Alaska Coastal Current
C. Douglas
ALASKA PENINSULA
Shelikof Strait North
Line 8
Shelikof Strait Exit
KODIAK I.
Sutwik Is.
Trinity Islands
Semidi Is.
Chirikof I.
Shumagin Is.
200
2000
Alaskan Stream
0 50 100 km
Depth in meters
60°N
59°
58°
57°
56°
55°
160°
159°
158°
157°
156°
155°
154°
153°
152°
151°
150°

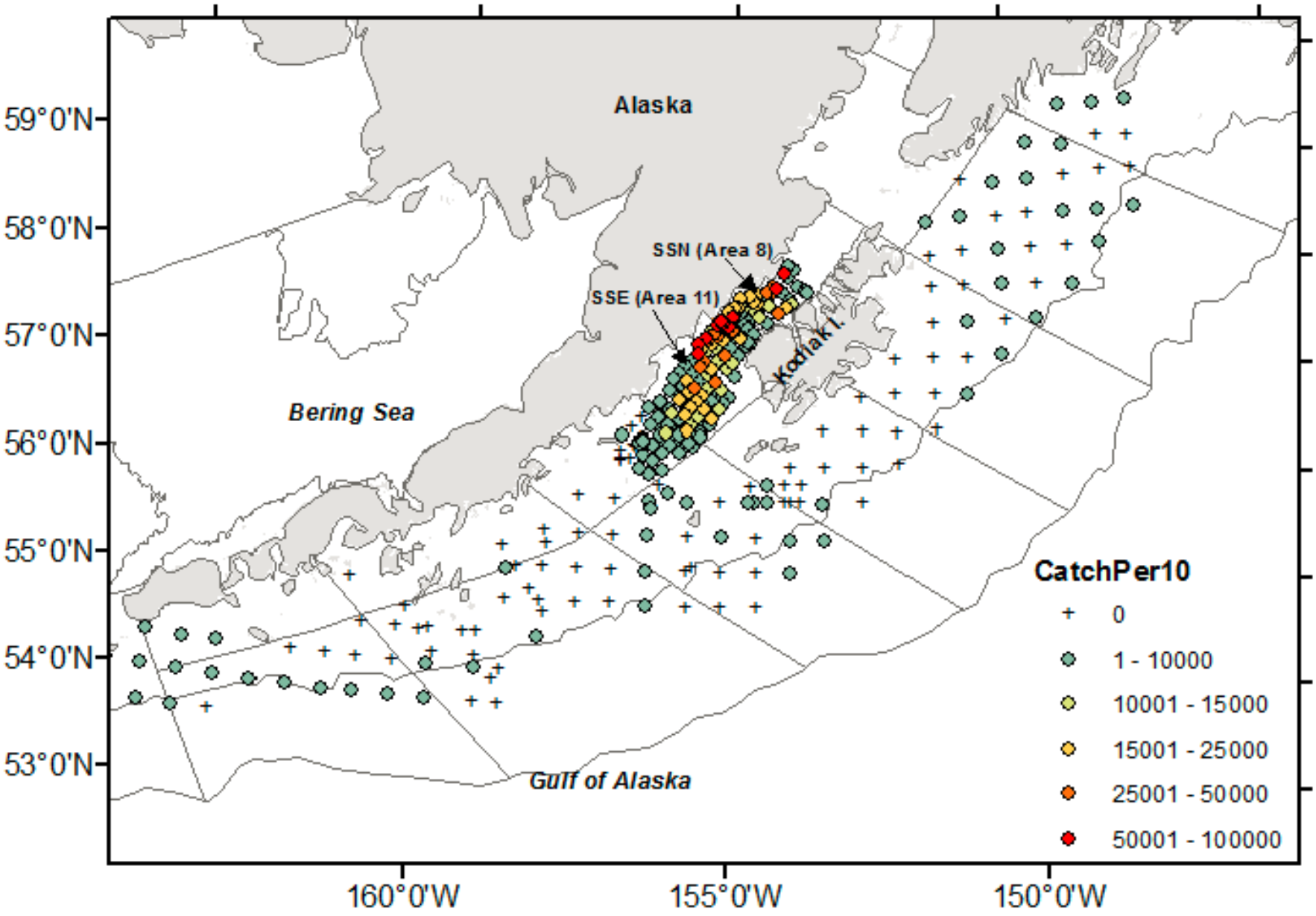
Alaska
Bering Sea
Gulf of Alaska
Kodiak I.
SSN (Area 8)
SSE (Area 11)
59°0'N
58°0'N
57°0'N
56°0'N
55°0'N
54°0'N
53°0'N
160°0'W
155°0'W
150°0'W
CatchPer10
0
1 - 10000
10001 - 15000
15001 - 25000
25001 - 50000
50001 - 100000

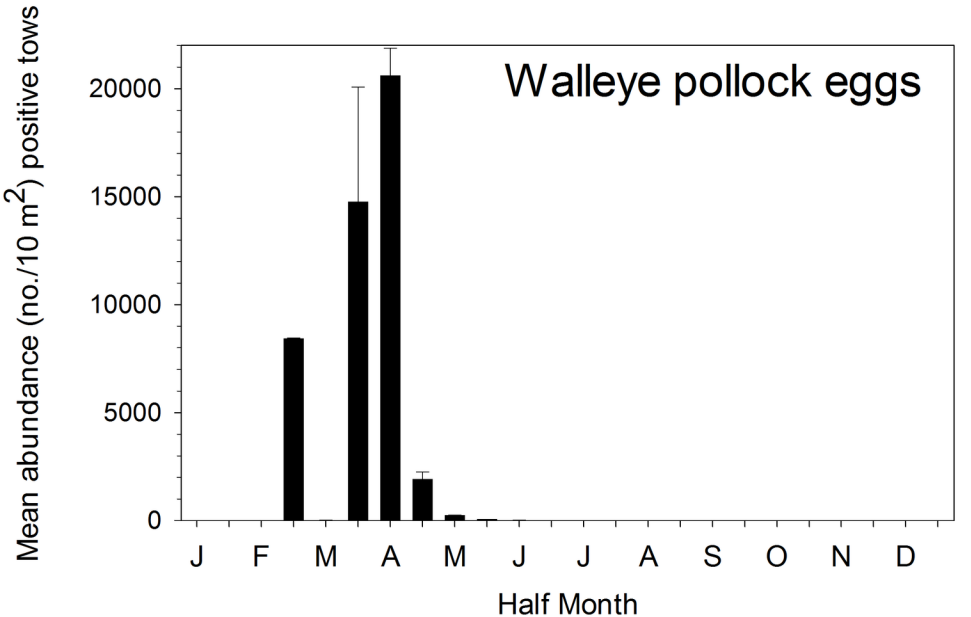
Walleye pollock eggs
Mean abundance (no./10 m2) positive tows
20000
15000
10000
5000
0
J
F
M
A
M
J
J
A
S
O
N
D
Half Month

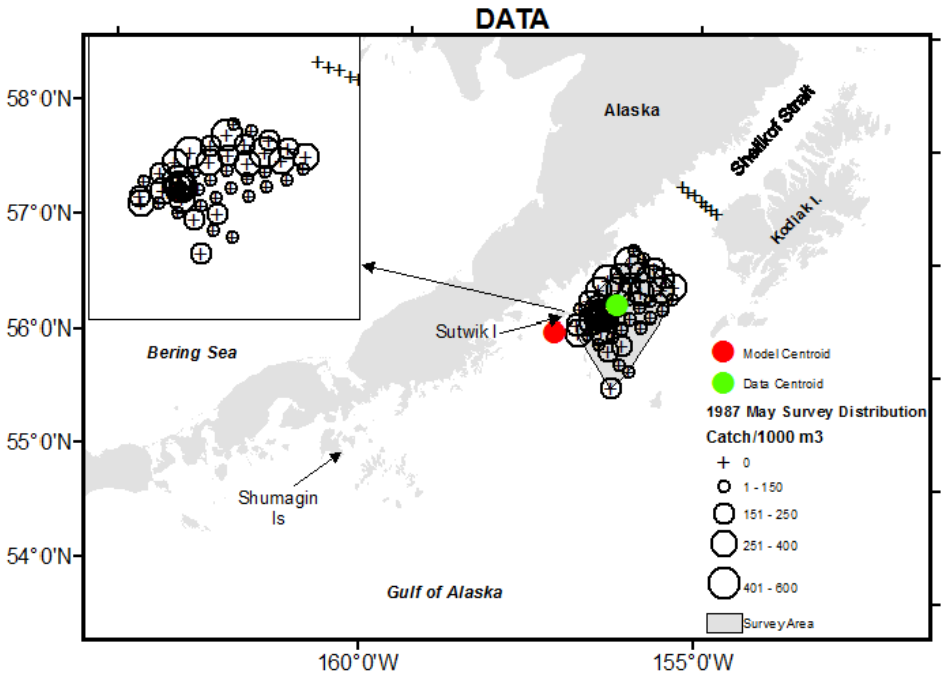
DATA
58° 0'N
57° 0'N
56° 0'N
55° 0'N
54° 0'N
160° 0'W
155° 0'W
Alaska
Shelikof Strait
Kodiak I.
Sutwik I
Bering Sea
Shumagin Is
Gulf of Alaska
Model Centroid
Data Centroid
1987 May Survey Distribution
Catch/1000 m3
0
1 - 150
151 - 250
251 - 400
401 - 600
Survey Area

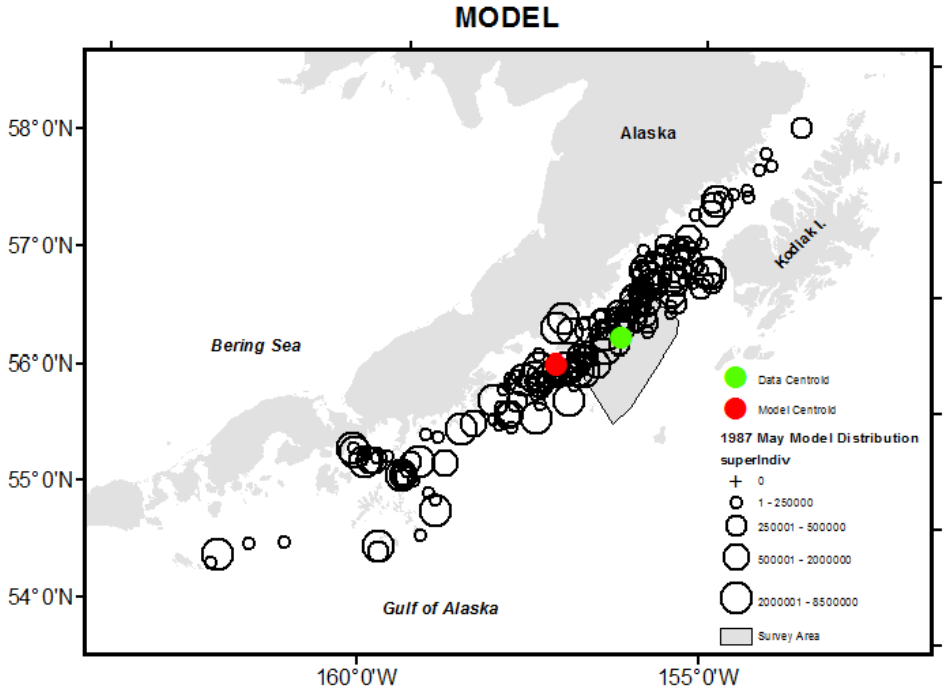
MODEL
58° 0'N
57° 0'N
56° 0'N
55° 0'N
54° 0'N
160° 0'W
155° 0'W
Alaska
Kodiak I.
Bering Sea
Gulf of Alaska
Data Centroid
Model Centroid
1987 May Model Distribution
superIndiv
0
1 - 250000
250001 - 500000
500001 - 2000000
2000001 - 8500000
Survey Area

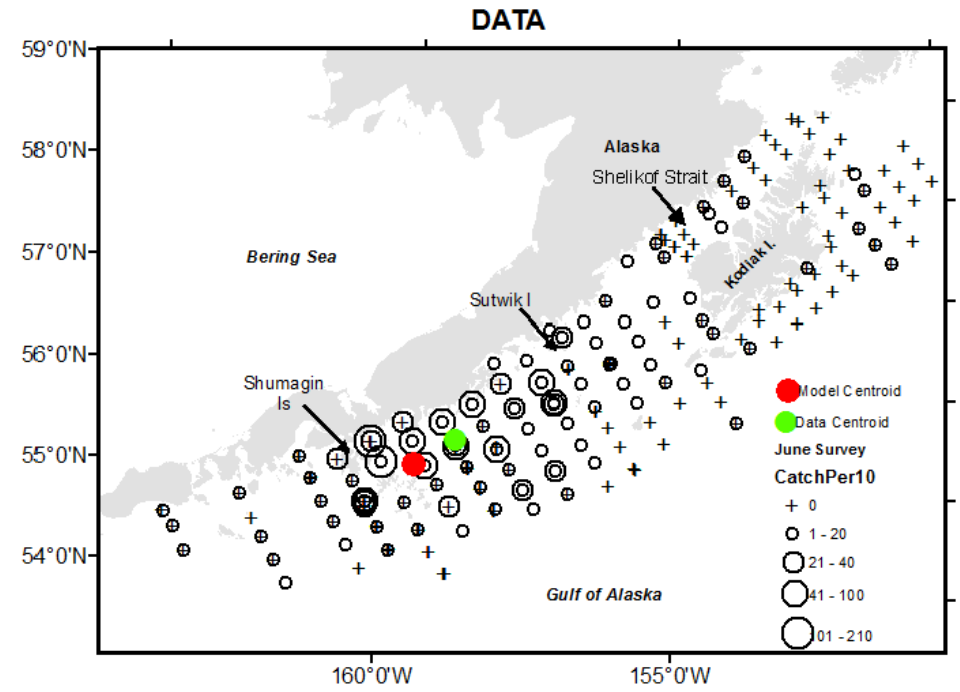
DATA
59°0'N
58°0'N
57°0'N
56°0'N
55°0'N
54°0'N
160°0'W
155°0'W
Alaska
Shelikof Strait
Bering Sea
Kodiak I.
Sutwik I
Shumagin Is
Gulf of Alaska
Model Centroid
Data Centroid
June Survey
CatchPer10
0
1 - 20
21 - 40
41 - 100
01 - 210

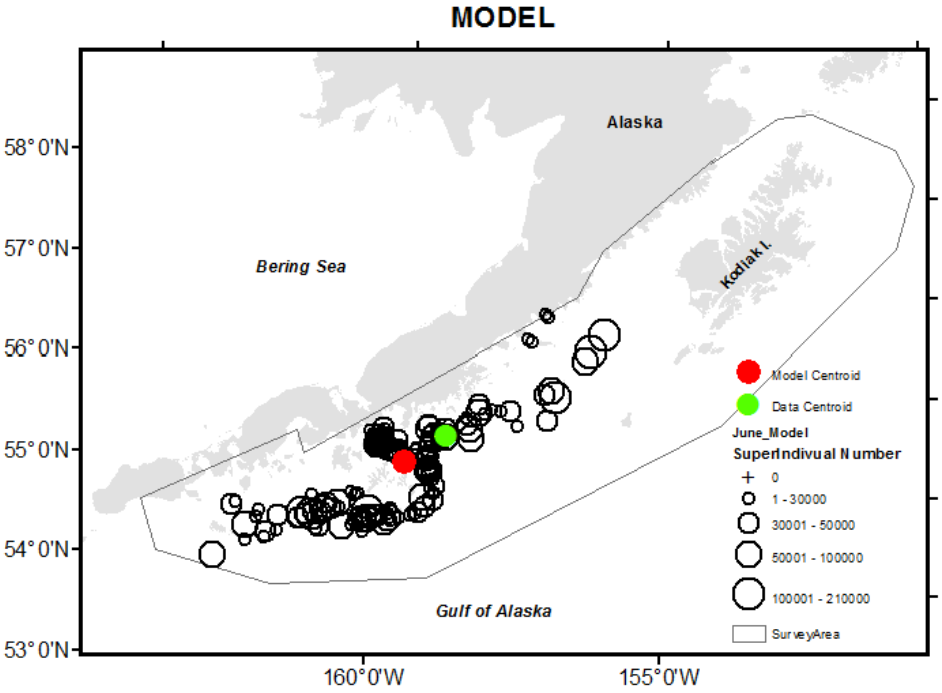
MODEL
58°0'N
57°0'N
56°0'N
55°0'N
54°0'N
53°0'N
160°0'W
155°0'W
Alaska
Bering Sea
Kodiak I.
Gulf of Alaska
Model Centroid
Data Centroid
June_Model
SuperIndivual Number
0
1 - 30000
30001 - 50000
50001 - 100000
100001 - 210000
SurveyArea

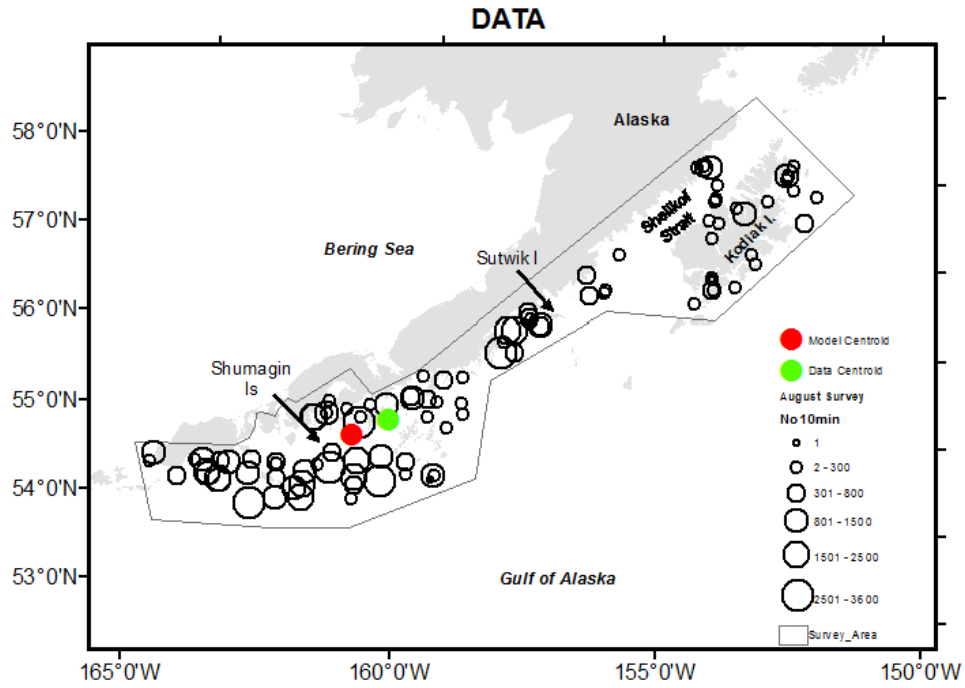
DATA
Alaska
Bering Sea
Gulf of Alaska
Sutwik I
Shelikof Strait
Kodiak I.
Shumagin Is
58°0'N
57°0'N
56°0'N
55°0'N
54°0'N
53°0'N
165°0'W
160°0'W
155°0'W
150°0'W
Model Centroid
Data Centroid
August Survey
No10min
1
2 - 300
301 - 800
801 - 1500
1501 - 2500
2501 - 3600
Survey_Area

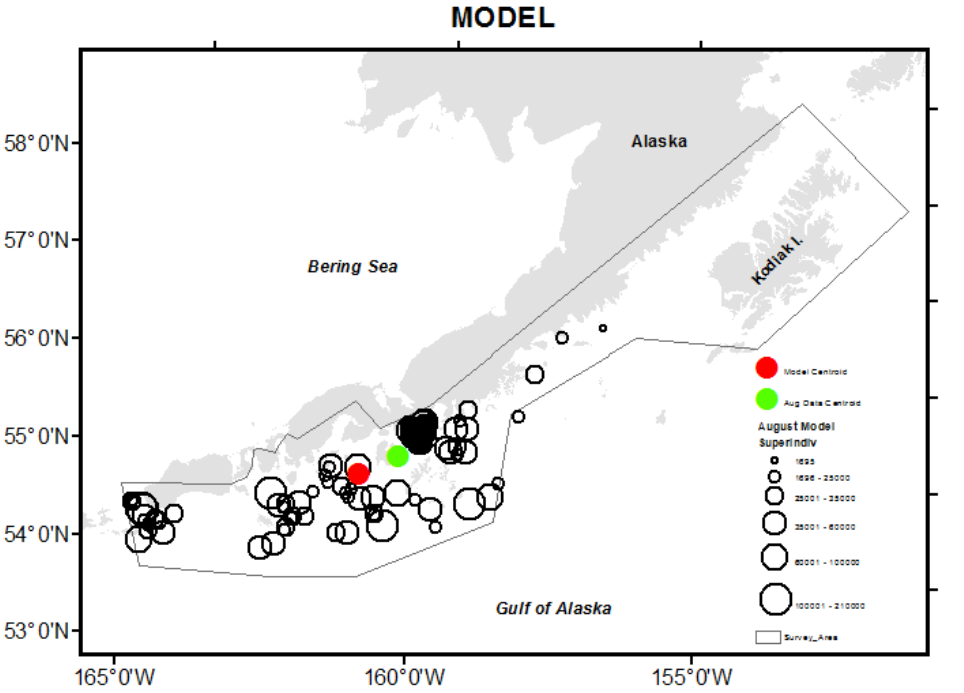
MODEL
Alaska
Bering Sea
Gulf of Alaska
Kodiak I.
58°0'N
57°0'N
56°0'N
55°0'N
54°0'N
53°0'N
165°0'W
160°0'W
155°0'W
Model Centroid
Aug Data Centroid
August Model
Superindiv
1695
1696 - 25000
25001 - 35000
35001 - 60000
60001 - 100000
100001 - 210000
Survey_Area

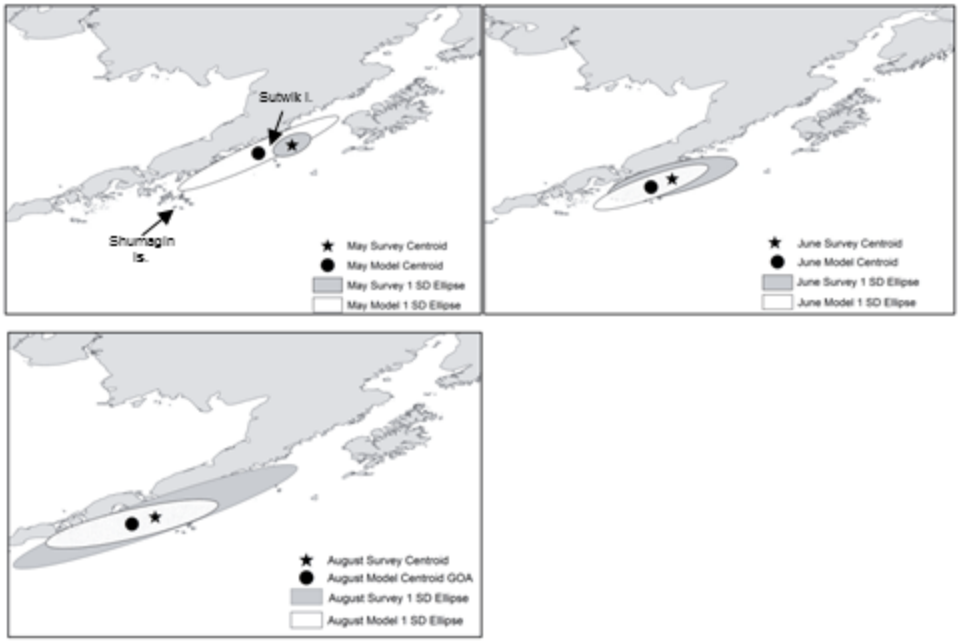
Sutwik I.
Shumagin Is.
May Survey Centroid
May Model Centroid
May Survey 1 SD Ellipse
May Model 1 SD Ellipse
June Survey Centroid
June Model Centroid
June Survey 1 SD Ellipse
June Model 1 SD Ellipse
August Survey Centroid
August Model Centroid GOA
August Survey 1 SD Ellipse
August Model 1 SD Ellipse

## DATA

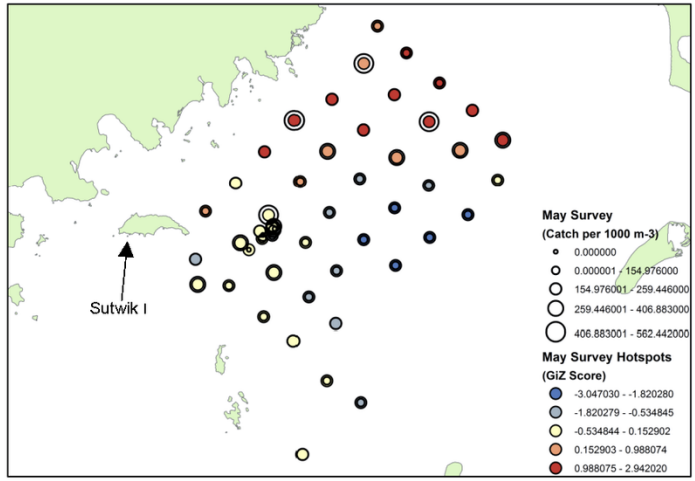
Sutwik I
May Survey
(Catch per 1000 m-3)
0.000000
0.000001 - 154.976000
154.976001 - 259.446000
259.446001 - 406.883000
406.883001 - 562.442000
May Survey Hotspots
(GiZ Score)
-3.047030 - -1.820280
-1.820279 - -0.534845
-0.534844 - 0.152902
0.152903 - 0.988074
0.988075 - 2.942020

## MODEL

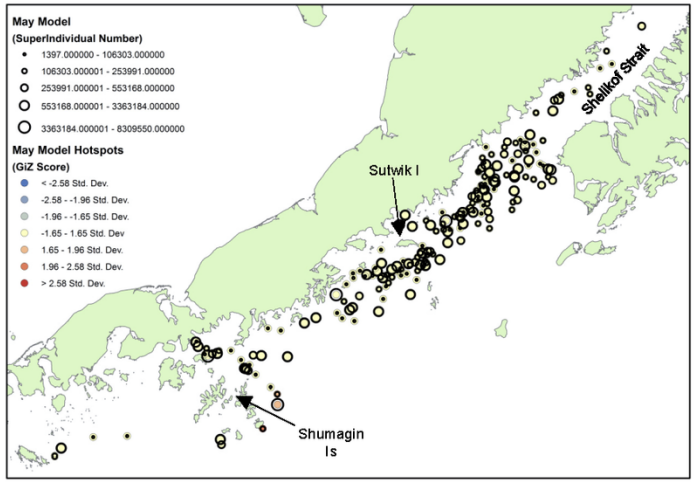
May Model
(SuperIndividual Number)
1397.000000 - 106303.000000
106303.000001 - 253991.000000
253991.000001 - 553168.000000
553168.000001 - 3363184.000000
3363184.000001 - 8309550.000000
May Model Hotspots
(GiZ Score)
< -2.58 Std. Dev.
-2.58 - -1.96 Std. Dev.
-1.96 - -1.65 Std. Dev.
-1.65 - 1.65 Std. Dev
1.65 - 1.96 Std. Dev.
1.96 - 2.58 Std. Dev.
> 2.58 Std. Dev.
Sutwik I
Shelikof Strait
Shumagin
Is

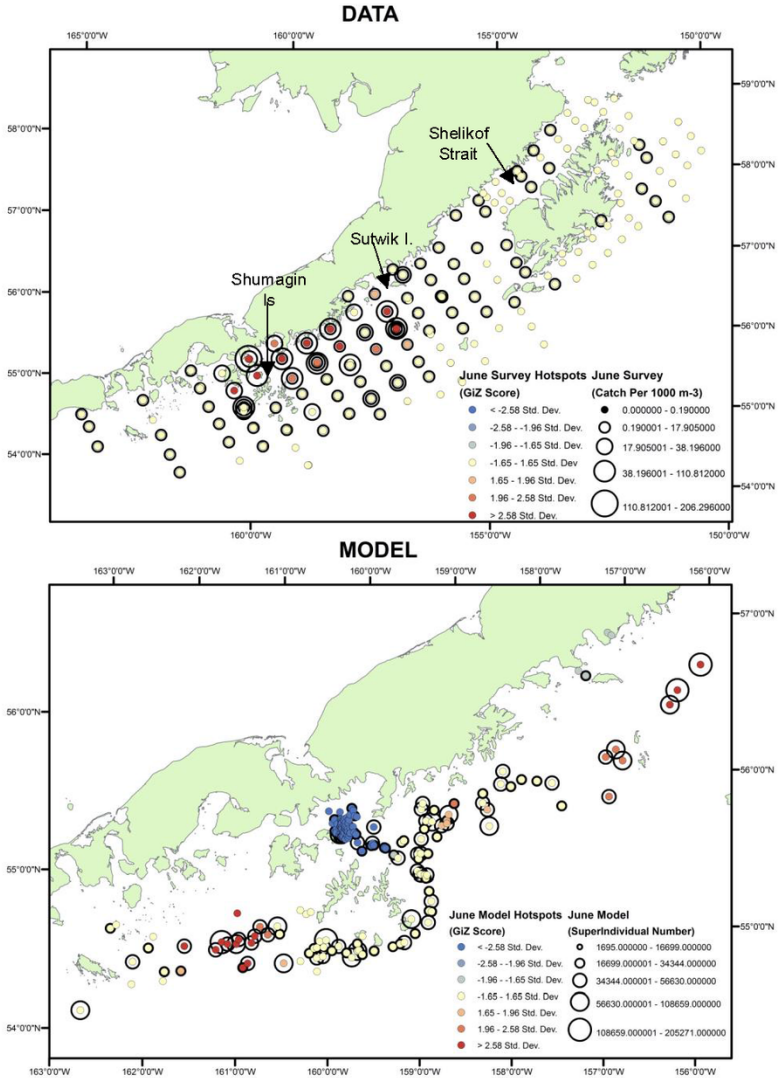
DATA
165°0'0"W
160°0'0"W
155°0'0"W
150°0'0"W
59°0'0"N
58°0'0"N
57°0'0"N
56°0'0"N
55°0'0"N
54°0'0"N
Shelikof Strait
Sutwik I.
Shumagin Is
June Survey Hotspots (GiZ Score)
< -2.58 Std. Dev.
-2.58 - -1.96 Std. Dev.
-1.96 - -1.65 Std. Dev.
-1.65 - 1.65 Std. Dev
1.65 - 1.96 Std. Dev.
1.96 - 2.58 Std. Dev.
> 2.58 Std. Dev.
June Survey (Catch Per 1000 m-3)
0.000000 - 0.190000
0.190001 - 17.905000
17.905001 - 38.196000
38.196001 - 110.812000
110.812001 - 206.296000
MODEL
163°0'0"W
162°0'0"W
161°0'0"W
160°0'0"W
159°0'0"W
158°0'0"W
157°0'0"W
156°0'0"W
57°0'0"N
56°0'0"N
55°0'0"N
54°0'0"N
June Model Hotspots (GiZ Score)
< -2.58 Std. Dev.
-2.58 - -1.96 Std. Dev.
-1.96 - -1.65 Std. Dev.
-1.65 - 1.65 Std. Dev
1.65 - 1.96 Std. Dev.
1.96 - 2.58 Std. Dev.
> 2.58 Std. Dev.
June Model (SuperIndividual Number)
1695.000000 - 16699.000000
16699.000001 - 34344.000000
34344.000001 - 56630.000000
56630.000001 - 108659.000000
108659.000001 - 205271.000000

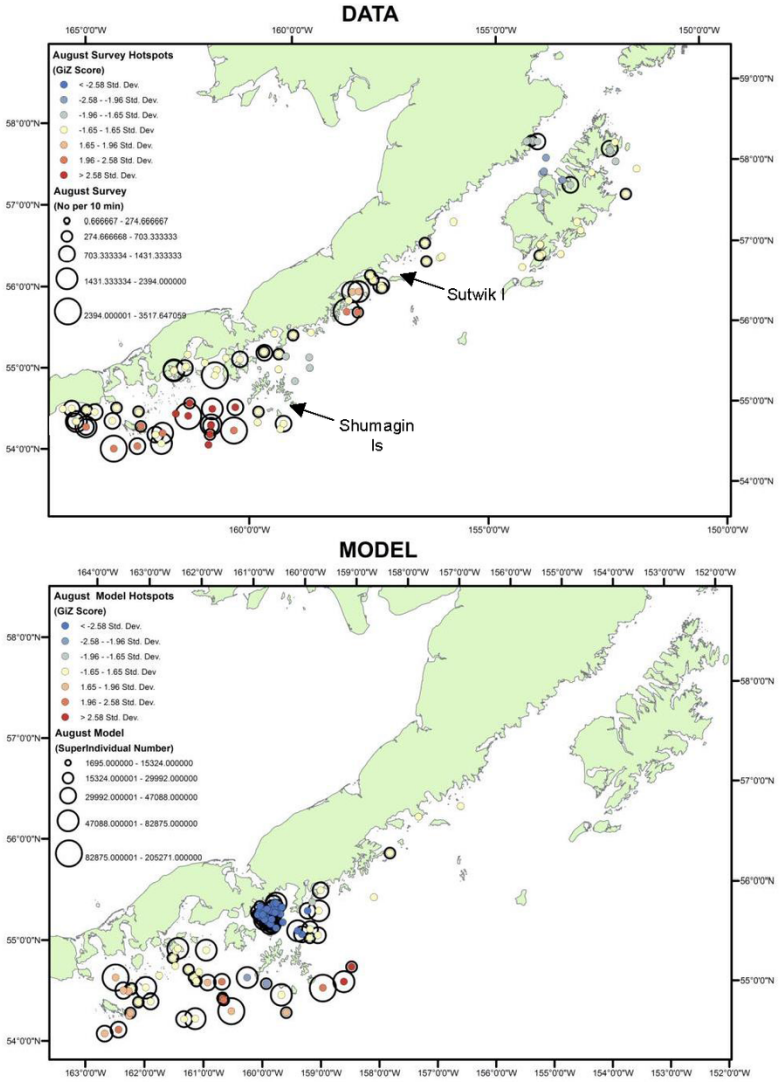
DATA
August Survey Hotspots
(GiZ Score)
< -2.58 Std. Dev.
-2.58 - -1.96 Std. Dev.
-1.96 - -1.65 Std. Dev.
-1.65 - 1.65 Std. Dev
1.65 - 1.96 Std. Dev.
1.96 - 2.58 Std. Dev.
> 2.58 Std. Dev.
August Survey
(No per 10 min)
0.666667 - 274.666667
274.666668 - 703.333333
703.333334 - 1431.333333
1431.333334 - 2394.000000
2394.000001 - 3517.647059
Sutwik I
Shumagin Is
MODEL
August Model Hotspots
(GiZ Score)
< -2.58 Std. Dev.
-2.58 - -1.96 Std. Dev.
-1.96 - -1.65 Std. Dev.
-1.65 - 1.65 Std. Dev
1.65 - 1.96 Std. Dev.
1.96 - 2.58 Std. Dev.
> 2.58 Std. Dev.
August Model
(SuperIndividual Number)
1695.000000 - 15324.000000
15324.000001 - 29992.000000
29992.000001 - 47088.000000
47088.000001 - 82875.000000
82875.000001 - 205271.000000

Bin size = 1/4°

Bin size = 1/2°

Bin size = 3/4°

May
Latitude

June-July
Latitude

Aug-Sep
Latitude

NDI=3245.5

NDI=194.3

NDI=132.4

NDI=7903.8

NDI=4733.6

NDI=835.1

NDI=8843

NDI=6971.2

NDI=1620.5

60°N
59°N
58°N
57°N
56°N
55°N
54°N

163°W
160°W
157°W
154°W
151°W

Longitude

1000
800
600
400
200
0
-200
-400
-600
-800
-1000

500
400
300
200
100
0
-100
-200
-300
-400
-500

Bin size = 1/4°

Bin size = 1/2°

Bin size = 3/4°

May
Latitude

June-July
Latitude

Aug-Sep
Latitude

60°N
59°N
58°N
57°N
56°N
55°N
54°N

C=0.03

C=0.08

C=0.14

C=0.2

C=0.07

C=0.12

C=0.02

C=0.01

C=0.02

163°W
160°W
157°W
154°W
151°W

Longitude

1
0.9
0.8
0.7
0.6
0.5
0.4
0.3
0.2
0.1

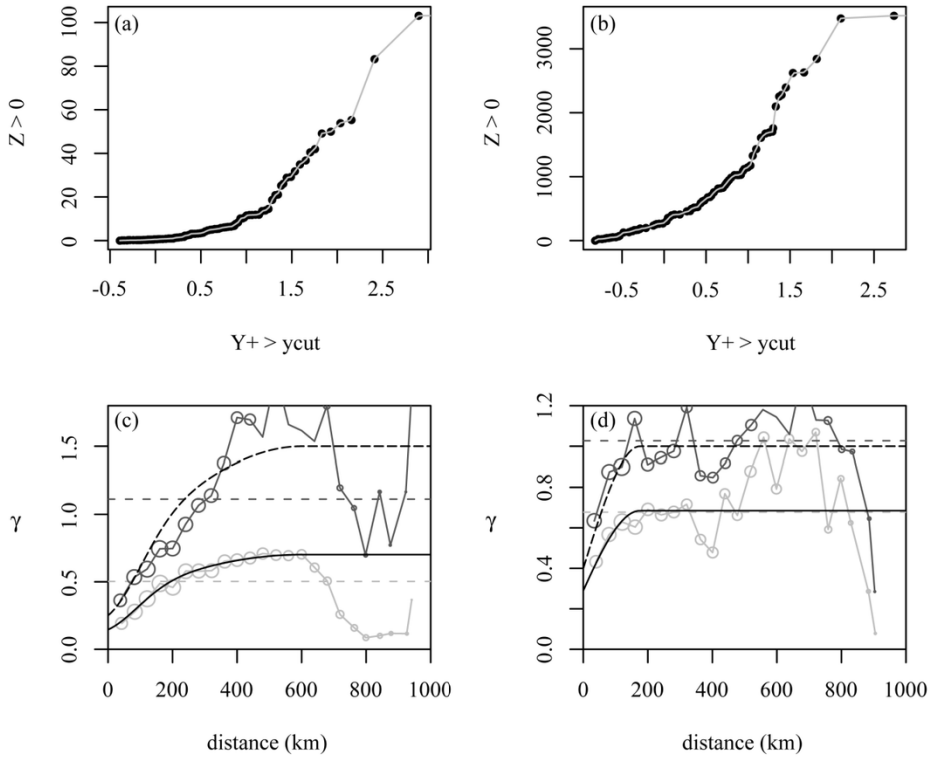
(a)
Z > 0
0 20 40 60 80 100
-0.5 0.5 1.5 2.5
Y+ > ycut
(b)
Z > 0
0 1000 2000 3000
-0.5 0.5 1.5 2.5
Y+ > ycut
(c)
γ
0.0 0.5 1.0 1.5
0 200 400 600 800 1000
distance (km)
(d)
γ
0.0 0.4 0.8 1.2
0 200 400 600 800 1000
distance (km)

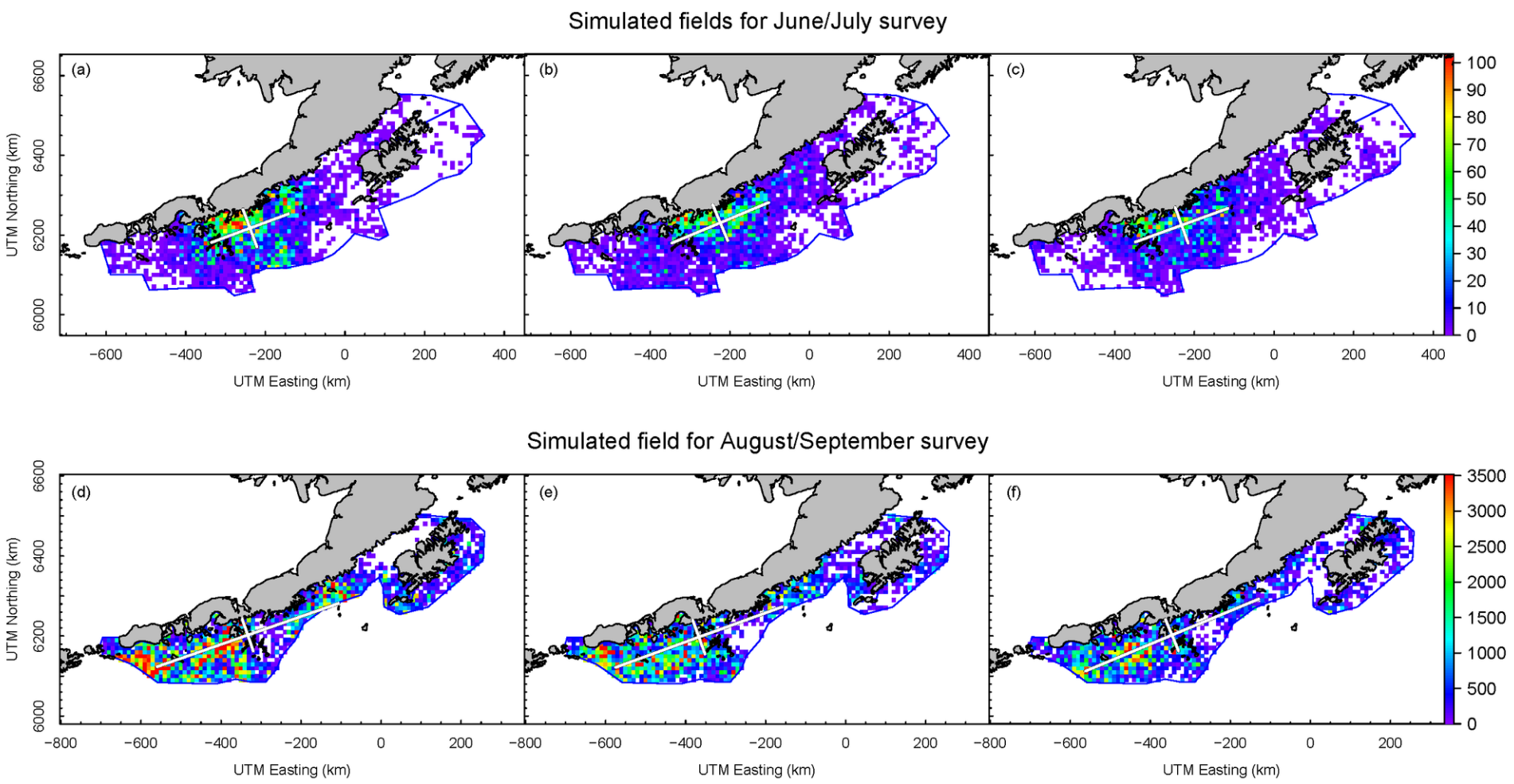
Simulated fields for June/July survey
(a)
(b)
(c)
UTM Northing (km)
6000
6200
6400
6600
−600
−400
−200
0
200
400
UTM Easting (km)
0
10
20
30
40
50
60
70
80
90
100
Simulated field for August/September survey
(d)
(e)
(f)
−800
−600
−400
−200
0
200
UTM Easting (km)
0
500
1000
1500
2000
2500
3000
3500